

Finite-amplitude gravity waves in the atmosphere: traveling wave solutions

Mark Schlutow¹†, R. Klein¹ and U. Achatz²

¹Institut für Mathematik, Freie Universität Berlin, Arnimallee 6, 14195 Berlin, Germany

²Institut für Atmosphäre und Umwelt, Goethe-Universität Frankfurt, Altenhöferallee 1, 60438 Frankfurt am Main, Germany

(Received xx; revised xx; accepted xx)

Wentzel-Kramers-Brillouin (WKB) theory was employed by Grimshaw (Geophys. Fluid Dyn., **6**, 131–148, 1974) and Achatz et al. (JFM, **210**, 120–147, 2010) to derive modulation equations for non-hydrostatic internal gravity wave packets in the atmosphere. This theory allows for wave packet envelopes with vertical extent comparable to the pressure scale height and for large wave amplitudes with wave-induced mean flow speeds comparable to the local fluctuation velocities.

Two classes of exact traveling wave solutions to these nonlinear modulation equations are derived here. The first class involves horizontally propagating wave packets superimposed over rather general background states. In a co-moving frame of reference, examples from this class have a structure akin to stationary mountain lee waves. Numerical simulations corroborate the existence of close-by traveling wave solutions under the pseudo-incompressible model and reveal better than expected convergence with respect to the asymptotic expansion parameter.

Traveling wave solutions of the second class also feature a vertical component of their group velocity but exist under isothermal background stratification only. These waves include an interesting nonlinear wave-meanflow interaction process: A horizontally periodic wave packet propagates vertically while draining energy from the mean wind aloft. In the process it decelerates the lower level wind. It is shown that the modulation equations equally apply for hydrostatic waves in the limit of large horizontal wavelengths.

Aside from these results of direct physical interest, the new nonlinear traveling wave solutions provide a firm basis for subsequent studies of nonlinear internal wave instability and for the design of subtle test cases for numerical flow solvers.

Key words:

1. Introduction

The stratification of the earth’s atmosphere gives rise to internal gravity waves which obtain kinetic energy and momentum from the mean flow when excited, transport them vertically as well as horizontally, and redistribute them by non-linear interaction and breaking. By these processes, gravity waves have a major impact on the large-scale middle atmospheric circulation (Fritts 2003; Becker 2012). In fact, when wave packets propagate upwards in a density-stratified medium they amplify and ultimately tend to break, generate turbulence, and transfer heat and momentum to the mean flow. At the

† Email address for correspondence: mark.schlutow@fu-berlin.de

same time, internal waves appear on a considerable spectrum of wavelengths, so that even high resolution numerical models can only resolve the long-wave part of this spectrum whereas the small-scale part together with the effects of wave breaking and turbulence need to be parametrized (McLandress 1998; Alexander & Dunkerton 1999).

In developing such parameterizations it is observed that wave breaking and the subsequently developing turbulence are the result of wave instabilities. Numerous different instability mechanisms are known and provide wave breaking criteria in gravity wave parameterizations. Specifically, these schemes aim to predict those positions where wave drag is produced and affects the mean flow, e.g.: if the perturbation of the background state due to a wave leads to unstable stratification locally, then the wave is said to be statically unstable. Yet, even statically stable waves can generate strongly growing modes and become unstable subsequently if their local Richardson number is less than a quarter (Lelong & Dunkerton 1998; Achatz 2007; Liu *et al.* 2010).

By means of Floquet theory, which is applicable for linear partial differential equations with periodic coefficients, parametric instabilities were considered by Mied (1976), Lombard & Riley (1996) and others. These authors exploited that monochromatic plane waves in a uniformly stratified background are exact solutions of the Boussinesq equations that are nonlinear in a particular way. More recently, effects of modulational instability in a weakly nonlinear regime, in which wave-induced mean flows are of the order of the wave-amplitude squared, were analyzed by Sutherland (2001, 2006) and Tabaei & Akylas (2007).

The underlying basis for analytical stability studies are traveling wave solutions. They are defined as stationary wave-like solutions in a translational coordinate system moving with a constant relative velocity. The aforementioned plane waves are prime examples of this kind. Once traveling wave solutions are found, linearization of the chosen fluid flow equation system relative to these stationary solutions generates an eigenvalue problem. If the spectrum of the resulting linear operator exhibits a positive real part, then the traveling wave solution is linearly unstable.

All above-mentioned stability analyses assume a Boussinesq-type fluid. While this is appropriate for small-scale flows, it is of limited value for flows covering scales comparable to the pressure scale height or larger. Thus, Klein *et al.* (2010); Klein (2011); Achatz *et al.* (2010) discuss the validity of various flow models for the description of internal wave dynamics in comparison with the full compressible Euler equations. They found that, in this sequence, the Boussinesq, anelastic, pseudo-incompressible, and full compressible flow equations have an increasing range of validity.

In particular, Achatz *et al.* (2010) presented a theory that simultaneously covers (i) finite amplitude, (ii) nonlinear wave packets with (iii) wave envelopes extending over a pressure scale height or more in (iv) strong, non-uniform stratification. This is of interest, e.g., in studying breaking waves in the stratosphere. The theory is derived from the full compressible flow equations through a multiple-scales approach combined with Wentzel-Kramer-Brillouin (WKB) theory that assumes slow variation of the wave envelope and phase. Out of the family of sound-proof models (Boussinesq, anelastic, pseudo-incompressible), only the latter covers this and all the less demanding regimes and yields results in all of them that are identical to leading order with those obtained from the full compressible model. In this sense, this theory is, to the best of the authors' knowledge, the most general description of internal wave packets in the atmosphere currently available, and is thus adopted as the basis for the present work. The theory was tested favourably against numerical simulations by Rieper *et al.* (2013a).

The main motivation for the present work is to prepare the ground for internal wave stability analysis of internal wave packets in a deep atmosphere covering at least a

pressure scale height and for the development of related subgrid scale parameterizations. To this end we derive traveling wave solutions of the large scale WKB equations derived by Achatz *et al.* (2010) as references for linearizations. Being exact solutions of a nonlinear flow model valid in a physically relevant regime, however, these solutions may also be of interest independently of the stability question: The horizontally traveling wave solutions strongly resemble mountain lee waves in their co-moving frame of reference, so that the present theory may provide a new analytical handle to study nonlinear properties of the latter. The class of vertically traveling wave solutions includes narrowly supported structures that redistribute the kinetic energy of the background flow to produce propagating shock-like transitions with strong vertical shear somewhat reminiscent of the wave patterns that induce the QBO, albeit on much larger horizontal scales (Baldwin *et al.* 2001). Our main focus here is on the small-scale part of the spectrum, however, so that we defer more detailed analyses of larger scale flows by related methods to future work.

This paper is structured as follows. In §2 we will revisit the scaling assumptions of Achatz *et al.* (2010) to derive the governing equations. A spectral WKB ansatz for finite-amplitude waves will be exploited in §3. We will examine, in addition to that, the existence of weak asymptotic solutions. This will lift the already well established theory on a stronger mathematical basis. Solvability constraints for the ansatz functions lead to the modulation equations predicting the evolution of the wave properties. In §4 we will investigate the energy budget of the wave-mean-flow interaction and show that the modulation equations conserve the sum of wave and mean-flow energy which allows to compute an energy exchange rate. §5 contains our main results. Here, we derive traveling wave solutions for the modulation equations by means of a translational coordinate transformation. These traveling waves give us leading order solutions for the governing equations. We will find two distinct classes of traveling wave solutions. For the first one, we will present an analytic solution and for the second one we can show the structure of the wave and for which initial conditions and set of parameters a solution exists. The exact traveling wave solutions are asymptotic solutions to the fully nonlinear Euler equations. We will test the validity of the solutions with respect to the Euler dynamics numerically in §6. In §7 we will show consistency of hydrostatic gravity waves with the modulation equations. The paper will be concluded with some final remarks in §8.

2. The governing equations

In this section we will present a derivation of equations, that describes the dynamics of saturated gravity waves in a hydrostatic background flow, starting from the dimensionless Euler equations.

2.1. Scaling the Euler equations for large amplitude internal waves

We consider gravity waves in a two-dimensional domain neglecting the Coriolis force. Viscous effects as well as external heating sources are ignored, too. With respect to these basic assumptions the time evolution of the flow is governed by the compressible Euler equations for an ideal gas which may be written in non-dimensionalized form as

$$\begin{aligned}
 0 &= D_t \mathbf{v} + \frac{1-\kappa}{\kappa} \frac{1}{\text{Ma}^2} \theta \nabla \pi + \frac{1}{\text{Fr}^2} \mathbf{e}_z \\
 0 &= D_t \theta \\
 0 &= D_t \pi + \frac{\kappa}{1-\kappa} \pi \nabla \cdot \mathbf{v}
 \end{aligned} \tag{2.1}$$

| | | | | | | |
|------------------------|------------------|------------------|---------------------------------|------------------|------------------|------------------|
| Dimensionless variable | x | z | t | \mathbf{v} | T | p |
| Reference value | L_{ref} | L_{ref} | $L_{\text{ref}}/v_{\text{ref}}$ | v_{ref} | T_{ref} | p_{ref} |
| Dimension in SI units | m | m | s | ms^{-1} | K | Pa |

TABLE 1. Non-dimensionalization of variables

with (x, z) the horizontal and vertical coordinate and the corresponding unit vectors \mathbf{e}_x and \mathbf{e}_z . Here, $D_t = \partial_t + \mathbf{v} \cdot \nabla$ is the material derivative. The velocity vector field is denoted by \mathbf{v} . The Exner pressure is related to the usual pressure by

$$\pi = p^\kappa \quad (2.2)$$

where $\kappa = 2/7$ is the ratio of the ideal gas constant R and the specific heat capacity at constant pressure c_p . From the temperature T we define the potential temperature to be

$$\theta = T/\pi. \quad (2.3)$$

The independent and dependent variables are non-dimensionalized according to table 1. The Mach and the Froude number are given by $\text{Ma} = v_{\text{ref}}/C_s$ and $\text{Fr} = v_{\text{ref}}/\sqrt{gL_{\text{ref}}}$ with

$$C_s = \sqrt{\frac{1}{1-\kappa}RT_{\text{ref}}} \quad (2.4)$$

the speed of sound and g the gravitational acceleration. Let $H_p, H_\theta, L_{\text{ref}}$, and N_{ref} denote the pressure and potential temperature scale height, a typical wavelength, and reference Brunt-Väisälä frequency, respectively. The distinguished asymptotic limit adopted by Grimshaw (1974) and Achatz *et al.* (2010) is reproduced by assuming:

(i) low Mach number

$$\sqrt{\frac{\kappa}{1-\kappa}} \text{Ma} = \varepsilon \ll 1, \quad (2.5)$$

(ii) leading-order stable stratification

$$\frac{H_p}{\Theta} \frac{d\bar{\Theta}}{dz} = O(1) \quad (\varepsilon \rightarrow 0) \quad \text{where} \quad H_p = \frac{RT_{\text{ref}}}{g} \approx 10 \text{ km}, \quad (2.6)$$

(iii) non-hydrostatic motions

$$x_{\text{ref}} = z_{\text{ref}} \equiv L_{\text{ref}} \approx 4 \text{ km}, \quad (2.7)$$

(iv) large internal wave Froude number

$$\text{Fr}_{\text{int}} = \frac{v_{\text{ref}}}{N_{\text{ref}}L_{\text{ref}}} = O(1) \quad (\varepsilon \rightarrow 0) \quad \text{where} \quad N_{\text{ref}} = \sqrt{\frac{g}{\Theta} \frac{d\bar{\Theta}}{dz}} \approx 0.02 \text{ Hz}. \quad (2.8)$$

On account of (2.5), (2.6), and (2.8) we find that $L_{\text{ref}}/H_p = O(\varepsilon)$ and we let

$$L_{\text{ref}} = \varepsilon H_\theta \quad \text{where} \quad H_\theta = H_p/\kappa \approx 40 \text{ km} \quad (2.9)$$

for specificity. Combining the scaling assumptions (i)–(iv), we obtain the distinguished limit $\text{Fr} = \varepsilon^{1/2}$ which links the Froude to the Mach number, so that ε is the only parameter appearing in (2.1).

2.2. Asymptotic scalings

Here we prepare the ground for the subsequent summary of the WKB analysis in section 3 by anticipating the essential spatio-temporal and amplitude scalings of the dependent variables from Achatz *et al.* (2010). Let

$$(X, Z, T) = (\varepsilon x, \varepsilon z, \varepsilon t) \quad (2.10)$$

denote compressed coordinates that resolve spatial scales comparable with the pressure scale height and the associated advection time scale. Furthermore, for any variable V , let

$$V_0(Z) \quad \text{and} \quad V_\varepsilon^{(i)}(x, z, t; \varepsilon) \quad (2.11)$$

denote its slowly varying leading-order horizontal background and the collection of its i th and higher order contributions in ε with wave-induced variations on the fast and slow scales. Then the asymptotic scaling of the WKB solutions to be discussed below can be summarized as

$$\begin{pmatrix} \mathbf{v} \\ \theta \\ \pi \end{pmatrix} = \begin{pmatrix} u_\varepsilon^{(0)}(x, z, t; \varepsilon) \\ w_\varepsilon^{(0)}(x, z, t; \varepsilon) \\ \theta_0(Z) + \varepsilon \theta_\varepsilon^{(1)}(x, z, t; \varepsilon) \\ \pi_0(Z) + \varepsilon^2 \pi_\varepsilon^{(2)}(x, z, t; \varepsilon) \end{pmatrix}. \quad (2.12)$$

In the velocity field the wave appears at $O(1)$, whereas potential temperature and Exner pressure decompose into leading-order hydrostatic background variations θ_0, π_0 satisfying

$$\frac{d\pi_0}{dZ} = -\frac{1}{\theta_0}, \quad (2.13)$$

and higher-order fluctuations. Potential temperature perturbations are of order $O(\varepsilon)$, whereas Exner pressure deviations appear first at $O(\varepsilon^2)$. See (Achatz *et al.* 2010) and section 3 below for more detail.

For later reference, we use the ideal gas equation of state to express the leading order density and temperature as

$$\rho_0 = \frac{\pi_0^{(1-\kappa)/\kappa}}{\theta_0} \quad (2.14)$$

and

$$T_0 = \theta_0 \pi_0, \quad (2.15)$$

respectively. In addition to that we also define the ‘‘logarithmic background derivative’’ of any $f_0 \in \{\theta_0, \pi_0, \rho_0, T_0\}$ by

$$\eta_f = \frac{1}{f_0} \frac{df_0}{dZ} = \frac{d \ln(f_0)}{dZ}. \quad (2.16)$$

Taking the derivative w.r.t. Z of (2.14) and substituting with (2.16) we find that

$$\frac{1-\kappa}{\kappa} \eta_\pi = \eta_\rho + \eta_\theta. \quad (2.17)$$

We can identify $\eta_\theta = N^2$ to be the local Brunt-Väisälä frequency squared, $-\eta_\rho^{-1}$ may be interpreted as the local density scale height. Combining (2.13) – (2.17) it turns out that

all background variables can be expressed by the background temperature,

$$\eta_\rho = -\eta_T - \frac{1}{\kappa T_0} \quad \text{and} \quad N^2 = \eta_T + \frac{1}{T_0}. \quad (2.18)$$

So, once the vertical background temperature profile is known, all profiles of the remaining background variables are determined. If we now inject the distinguished limit (2.9) as well as the multiple-scale representation from (2.12) into the Euler equations (2.1) and substitute by (2.17), we arrive at a system of evolution equations

$$\begin{aligned} D_t u + \partial_x P &= -\varepsilon NB \partial_x P \\ D_t w + \partial_z P - NB &= -\varepsilon (NB \partial_z P - N^2 P) + \varepsilon^2 N^3 BP \\ D_t B + Nw &= -\varepsilon (N^2 + \eta_N) w B \\ \partial_x u + \partial_z w &= -\varepsilon (N^2 + \eta_\rho) w + C \end{aligned} \quad (2.19)$$

for the new set of prognostic variables

$$U = (u, w, B, P)^T := \left(u_\varepsilon^{(0)}, w_\varepsilon^{(0)}, \frac{1}{N} \frac{\theta_\varepsilon^{(1)}}{\theta_0}, \theta_0 \pi_\varepsilon^{(2)} \right)^T \quad (2.20)$$

where B and P relate to the buoyancy and the kinetic pressure, respectively.

The expression

$$C = \varepsilon^2 (N^2 + \eta_\rho) \left(D_t P + \frac{\kappa}{1 - \kappa} P (\partial_x u + \partial_z w) \right) - \varepsilon^3 (N^2 + \eta_\rho) N^2 w P \quad (2.21)$$

in (2.19) denotes higher-order terms which do not contribute to the leading-order WKB solutions because either they are literally of higher order and just do not appear, or they do appear in the expanded equations up to the order considered but cancel each other. We note in passing that (2.19) without the C -terms constitutes Durran's pseudo-incompressible model equations, and this corroborates the conclusion by Achatz *et al.* (2010) that the full compressible and pseudo-incompressible models share the WKB-wave packet solutions in the considered flow regime. We will refer to system (2.19) henceforth as scaled Euler equations.

3. WKB theory for finite-amplitude gravity waves with non-uniform stratification

In this section we will apply a weak asymptotic scheme to derive the modulation equations whose traveling wave solutions are the main objective of this survey.

3.1. A spectral WKB expansion

The scaled Euler equations are a set of nonlinear, first-order PDEs whose coefficients depend only on the stretched coordinate Z due to the background stratification. To account for the nonlinearities we exploit an asymptotic spectral expansion approach

$$U = \sum_{n=0}^M \sum_{|m| \leq n+1} \varepsilon^n \hat{U}_{n,m} e^{im\varepsilon^{-1}\Phi} + o(\varepsilon^M) \quad (3.1)$$

for the vector (2.20). The subscript n keeps track of the order in ε while the m -subscript carries the order of the harmonics. So, resonant coupling of the wave with the mean flow, i.e. zeroth harmonics, occurs already in leading order (Chu & Mei 1970; Miura

& Kruskal 1974). We restrict $\hat{U}_{n,-m} = \hat{U}_{n,m}^*$ for real-valuedness, where $*$ indicates the complex conjugate of a variable. To account for the slowly varying background state we apply the WKB assumption that the coefficients and the phase are functions of only the slow variables (X, Z, T) , such that

$$(X, Z, T) \mapsto \hat{U}_{n,m}(X, Z, T), \quad \Phi(X, Z, T). \quad (3.2)$$

The differential operators become

$$\partial_t = \varepsilon \partial_T \quad \text{and} \quad \nabla = \varepsilon \nabla_\varepsilon = \varepsilon (\partial_X, \partial_Z)^T. \quad (3.3)$$

The phase should be also expanded in ε as well, like

$$\Phi = \Phi^{(0)} + \varepsilon^2 \Phi^{(2)} + O(\varepsilon^4). \quad (3.4)$$

We need only the even gauge functions because effects by any $\Phi^{(1)}$ are already captured by $\arg(\hat{U}_{0,1})$. Similarly, higher order odd phases are as well included in the corresponding coefficients. Since we will only analyze the system up to $M = 1$, these higher order effects do not matter in this work, so we keep simply $\Phi \equiv \Phi^{(0)}$. By means of (3.3) we can define the local wave vector and the frequency,

$$\omega = -\partial_T \Phi, \quad (3.5)$$

$$\mathbf{k} = \nabla_\varepsilon \Phi. \quad (3.6)$$

By inserting the ansatz (3.1) into the governing equations (2.19), we obtain an equation of the form

$$\sum_{k=0}^M \sum_{|l| \leq k+2} \varepsilon^k \mathcal{C}_{k,l}(X, Z, T) e^{i l \varepsilon^{-1} \Phi(X, Z, T)} + o(\varepsilon^M) = 0. \quad (3.7)$$

The coefficients $\mathcal{C}_{k,l}$ represent the terms which contain the ansatz functions $\hat{U}_{n,m}, \Phi$, their derivatives, and the background variables. One can now establish that in the limit $\varepsilon \rightarrow 0$ the coefficients must vanish independently of the order in ε and the order of the harmonics, i.e. $\mathcal{C}_{k,l} = 0$ for all possible k and l . The result is an equation hierarchy providing constraints on the ansatz functions which will give us the modulation equations. In order to achieve independence with regard to the harmonics Whitham (1965); Grimshaw (1974); Miura & Kruskal (1974); Tabaei & Akylas (2007) assumed *a priori* that the solution vector U is additionally to its spatio-temporal dependence also a periodic function of the fast phase $\varepsilon^{-1} \Phi$, so

$$U(\varepsilon^{-1} \Phi, X, Z, T; \varepsilon) = U(\varepsilon^{-1} \Phi + 2\pi, X, Z, T; \varepsilon). \quad (3.8)$$

If one now averages (3.7) with respect to the fast phase over a period 2π , then one can exploit that the harmonics are mutually orthogonal. In terms of this argument it was justified that the claim of independently vanishing coefficients must hold with regard to the average.

We encounter two issues, when we want to apply this technique to our approach in order to establish independently vanishing coefficients: (i) The fast phase depends on ε and (ii) it also depends itself on space and time. Due to these properties the assumption of periodicity must be justified in terms of the asymptotic series expansion of U . Miura & Kruskal (1974), who applied the nonlinear WKB method to the Korteweg-DeVries equation, wrote in this regard: ‘‘it remains unsettled whether or in what sense the series U [...] approximates the solution of the original problem.’’ However, we show in appendix A an alternative approach where periodicity is not needed by introducing the notion of

weak asymptotic solutions based on Danilov *et al.* (2003). It requires only that the ansatz functions are twice differentiable and it is hence more general than the averaging method. The key ideas to overcome the aforementioned issues are (i) to formulate (3.7) in a weak sense and (ii) to substitute the Cartesian coordinates by a map onto some phase following coordinates.

3.2. Leading-order analysis

In the following sections we present the equation hierarchy obtained by the weak asymptotic analysis. From $\mathcal{C}_{0,0} = 0$ we find solenoidality of the velocity field of the primary harmonics,

$$ik_x \hat{u}_{0,1} + ik_z \hat{w}_{0,1} = 0. \quad (3.9)$$

And constraints for some mean-flow components (the zeroth harmonics)

$$\hat{B}_{0,0} = \hat{w}_{0,0} = 0. \quad (3.10)$$

From $\mathcal{C}_{0,1} = 0$ we get a linear homogeneous system of equations for the primary harmonics

$$\mathbf{M}(-i\hat{\omega}, \mathbf{i}\mathbf{k}) \hat{U}_{0,1} = 0 \quad (3.11)$$

with the anti-Hermitian coefficient matrix

$$\mathbf{M}(-i\hat{\omega}, \mathbf{i}\mathbf{k}) = \begin{pmatrix} -i\hat{\omega} & 0 & 0 & ik_x \\ 0 & -i\hat{\omega} & -N & ik_z \\ 0 & N & -i\hat{\omega} & 0 \\ ik_x & ik_z & 0 & 0 \end{pmatrix}. \quad (3.12)$$

Here, $\hat{\omega} = \omega - \hat{u}_{0,0} k_x$ represents the intrinsic frequency that is the frequency one observes in a reference frame moving with the leading order mean flow. It differs from ω only by a Doppler-shift term. Equations $\mathcal{C}_{0,2} = 0$ hold by the same solenoidality (3.9).

3.3. First-order analysis

From $\mathcal{C}_{1,0} = 0$ we obtain next order constraints for the mean flow

$$\begin{aligned} \partial_T \hat{u}_{0,0} + \partial_X \hat{P}_{0,0} &= -\hat{u}_{0,1}^* \partial_X \hat{u}_{0,1} - \hat{w}_{0,1}^* \partial_Z \hat{u}_{0,1} \\ &\quad - ik_z \hat{u}_{0,1} \hat{w}_{1,1}^* - ik_z \hat{u}_{1,1} \hat{w}_{0,1}^* \\ &\quad - iNk_x \hat{B}_{0,1} \hat{P}_{0,1}^* + \text{c.c.}, \end{aligned} \quad (3.13)$$

$$\begin{aligned} (\partial_Z - N^2) \hat{P}_{0,0} - N \hat{B}_{1,0} &= -\hat{u}_{0,1}^* \partial_X \hat{w}_{0,1} - \hat{w}_{0,1}^* \partial_Z \hat{w}_{0,1} \\ &\quad - ik_x \hat{u}_{1,1} \hat{w}_{0,1}^* - ik_x \hat{u}_{0,1} \hat{w}_{1,1}^* \\ &\quad - iNk_z \hat{P}_{0,1} \hat{B}_{0,1}^* + \text{c.c.}, \end{aligned} \quad (3.14)$$

$$\begin{aligned} N \hat{w}_{1,0} &= -\hat{u}_{0,1}^* \partial_X \hat{B}_{0,1} - \hat{w}_{0,1}^* \partial_Z \hat{B}_{0,1} \\ &\quad - (N^2 + \eta_N) \hat{w}_{0,1}^* \hat{B}_{0,1} + \text{c.c.}, \end{aligned} \quad (3.15)$$

$$\partial_X \hat{u}_{0,0} = 0, \quad (3.16)$$

where c.c. stands for the complex conjugate of the previous terms. Primary harmonics are fixed by $\mathcal{C}_{1,1} = 0$: it follows a linear inhomogeneous system for $\hat{U}_{1,1}$,

$$\mathbf{M}(-i\hat{\omega}, \mathbf{i}\mathbf{k}) \hat{U}_{1,1} = -\mathbf{R}(\hat{U}_{1,2}, \mathbf{i}\mathbf{k}) \hat{U}_{0,-1} - \mathbf{L}(\delta_T, \nabla_\varepsilon) \hat{U}_{0,1} \quad (3.17)$$

with \mathbf{R} being a matrix

$$\mathbf{R}(\hat{U}_{1,2}, \mathbf{k}) = \begin{pmatrix} ik_x \hat{u}_{1,2} - ik_z \hat{w}_{1,2} & 2ik_z \hat{u}_{1,2} & 0 & 0 \\ 2ik_x \hat{w}_{1,2} & ik_z \hat{w}_{1,2} - ik_x \hat{u}_{1,2} & 0 & 0 \\ 2ik_x \hat{B}_{1,2} & 2ik_z \hat{B}_{1,2} & -ik_x \hat{u}_{1,2} - ik_z \hat{w}_{1,2} & 0 \\ 0 & 0 & 0 & 0 \end{pmatrix} \quad (3.18)$$

and \mathbf{L} being a linear differential operator

$$\mathbf{L}(\delta_T, \nabla_\varepsilon) = \begin{pmatrix} \delta_T & \partial_Z \hat{u}_{0,0} & 0 & \partial_X \\ 0 & \delta_T & 0 & \partial_Z - N^2 \\ 0 & 0 & \delta_T & 0 \\ \partial_X & \partial_Z + N^2 + \eta_\rho & 0 & 0 \end{pmatrix} \quad (3.19)$$

with $\delta_T = \partial_T + \hat{u}_{0,0} \partial_X + ik_x \hat{u}_{1,0} + ik_z \hat{w}_{1,0}$. Equations $\mathcal{C}_{1,2} = \mathcal{C}_{1,3} = 0$ yield the solenoidality,

$$ik_x \hat{u}_{1,2} + ik_z \hat{w}_{1,2} = 0, \quad (3.20)$$

for the velocity field of the secondary harmonics.

3.4. Second-order analysis

From $\mathcal{C}_{2,0} = 0$ we obtain among others

$$\partial_X \hat{u}_{1,0} + (\partial_Z + N^2 + \eta_\rho) \hat{w}_{1,0} = 0. \quad (3.21)$$

Here, we have already used the solenoidality (3.9). At this point we want to stop the iteration as we found enough constraints to construct leading order solutions.

3.5. Derivation of the modulation equations

The objective of this section is to exploit solvability constraints from the asymptotic analysis (3.9)–(3.21) in order to derive a closed set of equations which we will denote as modulation equations. Equation (3.11) has non-trivial solution only if $\det(\mathbf{M}) = 0$ yielding the dispersion relation

$$\hat{\omega}^2 = \frac{N^2 k_x^2}{k_x^2 + k_z^2}. \quad (3.22)$$

Note that $\text{sgn}(\hat{\omega}) = \pm 1$ indicates two different branches of the solution. By definition (3.5), the dispersion relation is essentially a prognostic equation for Φ which is by definition (3.6) of the form of a Hamilton-Jacobi equation. We find a particular vector $\mathcal{U} \in \ker(\mathbf{M})$ providing the polarization relation

$$\mathcal{U}(\hat{\omega}, \mathbf{k}) = \left(-i \frac{k_z}{k_x} \frac{\hat{\omega}}{N}, i \frac{\hat{\omega}}{N}, 1, -i \frac{k_z}{k_x^2} \frac{\hat{\omega}^2}{N} \right)^T \quad (3.23)$$

which is exactly the same polarization one would obtain in Boussinesq theory. For a detailed discussion on polarization relations in different sound-proof approximations we refer to Davies *et al.* (2003). We deduce that $\text{rank}(\mathbf{M}) = 3$. Since hence $\dim(\ker(\mathbf{M})) = 1$, we get a general solution for (3.11) by

$$\hat{U}_{0,1} = A \mathcal{U}(\hat{\omega}, \mathbf{k}) \quad \text{where} \quad \hat{U}_{0,1} = (\hat{u}_{0,1}, \hat{w}_{0,1}, \hat{B}_{0,1}, \hat{P}_{0,1})^T \quad (3.24)$$

with a yet free complex valued scalar A , that we later refer to as wave amplitude. Note in particular that $\hat{B}_{0,1} \equiv A$. By means of solenoidality of the several harmonics in the velocity, (3.9) and (3.20), we can show that $\mathbf{R}(\hat{U}_{1,2}, \mathbf{k}) \hat{U}_{0,-1} = 0$ which simplifies (3.17).

A necessary condition for the solvability of (3.17) is that any vector $\mathbf{L}\hat{U}_{0,1} \in \text{img}(\mathbf{M})$ has to be orthogonal to every $\mathcal{U} \in \ker(\mathbf{M})$ by the Rank-nullity theorem:

$$0 = \mathcal{U}^{*T} \mathbf{L}\hat{U}_{0,1}. \quad (3.25)$$

If equation (3.25) holds, then

$$0 = \hat{U}_{0,1}^{*T} \mathbf{L}\hat{U}_{0,1} + \text{c.c.} \quad (3.26)$$

$$0 = \hat{U}_{0,1}^{*T} \mathbf{L}\hat{U}_{0,1} - \text{c.c.} \quad (3.27)$$

must be true independently, if $A \neq 0$, which will serve to fix the degrees of freedom in

$$A = |A| \exp(i \arg(A)). \quad (3.28)$$

This argument essentially means that the real and the imaginary part of the rhs of (3.25) must vanish. Equation (3.26) is true if

$$\partial_T |A|^2 + (\nabla_\varepsilon + \eta_\rho \mathbf{e}_z) \cdot (\mathbf{c}_g |A|^2) + |A|^2 \frac{k_x}{\hat{\omega}} \frac{\partial \hat{\omega}}{\partial k_z} \partial_Z \hat{u}_{0,0} = 0 \quad (3.29)$$

which is derived using (3.16). This equation of motion yields essentially the evolution of the wave energy $\tilde{E} \equiv 2\rho_0 |A|^2$ that will be extensively discussed in §4. With the help of the consistency relations, $\partial_T \mathbf{k} + \nabla_\varepsilon \omega = 0$ and $\partial_X k_z = \partial_Z k_x$, that we obtain by cross differentiating the definitions (3.5) and (3.6), we find

$$(\partial_T + \mathbf{c}_g \cdot \nabla_\varepsilon) \hat{\omega} = -k_x \frac{\partial \hat{\omega}}{\partial k_z} \partial_Z \hat{u}_{0,0} \quad (3.30)$$

with the group velocity

$$\mathbf{c}_g = \frac{\partial \hat{\omega}}{\partial \mathbf{k}} + \hat{u}_{0,0} \mathbf{e}_x. \quad (3.31)$$

Combining $\rho_0 \times (3.29)$ with (3.30) and exploiting that $\rho_0 (\partial_Z + \eta_\rho) \cdot = \partial_Z (\rho_0 \cdot)$ result in a conservation law

$$\partial_T \mathcal{A} + \nabla_\varepsilon \cdot (\mathbf{c}_g \mathcal{A}) = 0, \quad (3.32)$$

for the wave action density $\mathcal{A} = \tilde{E} / \hat{\omega}$.

Let us return to the orthogonality of the kernel vector and the image vector (3.25). Exploiting (3.27) gives an equation of motion for the argument of A being basically some slow phase in addition to the fast phase $\varepsilon^{-1} \Phi$, i.e.

$$(\partial_T + \mathbf{c}_g \cdot \nabla_\varepsilon) \arg(A) = -k_x \hat{u}_{1,0} \quad (3.33)$$

which contains the first order mean-flow horizontal wind. With the aid of the derivations from above, we can handle the mean-flow equations (3.13)-(3.16), and (3.21). Using once more solenoidality from (3.9) and (3.20) it is possible to settle all the terms depending on $\hat{U}_{1,1}$, so

$$\partial_T \hat{u}_{0,0} + \partial_X \hat{P}_{0,0} = -\partial_X |\hat{u}_{0,1}|^2 - (\partial_Z + \eta_\rho) (\hat{u}_{0,1}^* \hat{w}_{0,1}) + \text{c.c.}, \quad (3.34)$$

$$\hat{w}_{1,0} = 0, \quad (3.35)$$

$$\partial_X \hat{u}_{0,0} = 0, \quad (3.36)$$

$$\partial_X \hat{u}_{1,0} = 0. \quad (3.37)$$

If we plug (3.24) into (3.34), we obtain an equation of motion for the leading order

mean-flow horizontal wind

$$\rho_0 \left(\partial_T \hat{u}_{0,0} + \partial_X \hat{P}_{0,0} \right) = -\nabla_\varepsilon \cdot \left((c_g - \hat{u}_{0,0} e_x) k_x \mathcal{A} \right). \quad (3.38)$$

The six equations (3.22), (3.32), (3.33), (3.36), (3.37), and (3.38), that we derived in this section, build a coupled system of equations for the six unknowns

$$\Phi, |A|, \arg(A), \hat{u}_{0,0}, \hat{P}_{0,0}, \text{ and } \hat{u}_{1,0}.$$

These are the aforementioned modulation equations. Once they are solved, the leading order, weak asymptotic solution of the scaled Euler equations has been found. It is worth mentioning that further solvability constraints for the first order mean flow will show up when we keep iterating the asymptotic scheme. The equations are in line with the calculations of Achatz *et al.* (2010). However in addition, we provide explicitly a prognostic equation for the slow phase $\arg(A)$ and a constraint for the first order mean-flow horizontal wind since they contribute to the leading order solution. Equation (3.14) containing $\hat{B}_{1,0}$ can be considered to be uncoupled as it does not affect neither the leading order solution nor does it appear in one of the other modulation equations.

4. Energy balance

An important aspect of wave dynamics is the energy budget. As our theory allows for a wave-mean-flow interaction, we want to investigate the energy exchange. We can rewrite (3.29) in terms of the wave energy density, which we may define as $\tilde{E} = 2\rho_0|A|^2$, so

$$\partial_T \tilde{E} + \nabla_\varepsilon \cdot (c_g \tilde{E}) = -c_{gz} k_x \mathcal{A} \partial_Z \hat{u}_{0,0}. \quad (4.1)$$

On the lhs we find a conservative flux, that transports energy with the group velocity, and on the rhs an energy source term that is associated with the vertical shear of the mean-flow horizontal wind. Let us now consider the mean-flow equation (3.38). Multiplying it by $\hat{u}_{0,0}$, using the chain rule and (3.16), give us an evolution equation for the mean-flow kinetic energy density $\bar{E} = \rho_0 \hat{u}_{0,0}^2 / 2$, so

$$\partial_T \bar{E} + \nabla_\varepsilon \cdot \left(\rho_0 \hat{u}_{0,0} \hat{P}_{0,0} e_x + c_{gz} k_x \mathcal{A} \hat{u}_{0,0} e_z \right) = c_{gz} k_x \mathcal{A} \partial_Z \hat{u}_{0,0}. \quad (4.2)$$

On the lhs we find also a conservative flux and on the rhs the same energy source term as in (4.1) but with the opposite sign making it an energy exchange rate. Because, if we add (4.1) and (4.2), we obtain a conservation law for the total energy density $E = \tilde{E} + \bar{E}$. We will refer to the energy exchange rate, i.e. the rhs of (4.2), as q . In conclusion, the total energy is conserved by the modulation equations. The sign of the exchange rate determines the direction of energy flow. E.g., an upward propagating wave packet with downward-facing phase speed vector transfers energy to the mean flow if the vertical shear is positive and vice versa.

5. Traveling wave solutions of the modulation equations

A key aspect for derivations of stability properties are traveling wave solutions. These are stationary, i.e. time-independent, solutions in a translational coordinate system moving with relative velocity \mathbf{C} . Performing a coordinate transformation of the governing equations and linearizing at the traveling wave solution results in an eigenvalue problem (due to the stationarity in the translational coordinates) for the time evolution of a small perturbation. The eigenvalues tell us whether the perturbation is bounded or whether it grows in time which implies instability. If we find traveling waves for the modulation

equations, we automatically obtain weak asymptotic traveling wave solutions for the scaled Euler equations. Consider the translational coordinate system $\Gamma = (\xi, \zeta, \tau)$ defined by the transformation $(X, Z, T) \mapsto \Gamma(X, Z, T)$:

$$\begin{pmatrix} \xi \\ \zeta \end{pmatrix} = \begin{pmatrix} X \\ Z \end{pmatrix} - \mathbf{C}T \text{ and } \tau = T, \quad (5.1)$$

with $\mathbf{C} = (C_x, C_z)^T$ being the constant relative velocity. Note that the unit vectors are preserved and the mapping is one-to-one. The nabla operator and the time derivative become

$$\nabla_\varepsilon = \mathbf{e}_x \partial_\xi + \mathbf{e}_z \partial_\zeta \quad (5.2)$$

and

$$\partial_T = \partial_\tau - \mathbf{C} \cdot \nabla_\varepsilon, \quad (5.3)$$

respectively. The modulation equations in the new coordinates may be written as

$$-(\partial_\tau - \mathbf{C} \cdot \nabla_\varepsilon)\Phi = \hat{\omega}(\mathbf{k}) + \hat{u}_{0,0}k_x, \quad (5.4)$$

$$(\partial_\tau - \mathbf{C} \cdot \nabla_\varepsilon)a + (\nabla_\varepsilon + \eta_\rho \mathbf{e}_z) \cdot (\mathbf{c}_g a) = 0, \quad (5.5)$$

$$(\partial_\tau + (\mathbf{c}_g - \mathbf{C}) \cdot \nabla_\varepsilon) \arg(A) = -k_x \hat{u}_{1,0}, \quad (5.6)$$

$$(\partial_\tau - C_z \partial_\zeta) \hat{u}_{0,0} + \partial_\xi \hat{P}_{0,0} = -(\nabla_\varepsilon + \eta_\rho \mathbf{e}_z) \cdot ((\mathbf{c}_g - \hat{u}_{0,0} \mathbf{e}_x) k_x a), \quad (5.7)$$

$$\partial_\xi \hat{u}_{0,0} = 0, \quad (5.8)$$

$$\partial_\xi \hat{u}_{1,0} = 0. \quad (5.9)$$

For the sake of the following arguments, we replaced \mathcal{A} by the ‘‘mass-specific’’ wave action density $a = \rho_0^{-1} \mathcal{A}$. These equations depend on the background variables N and η_ρ which are functions of $Z = \zeta + C_z \tau$ due to the transformation, so they depend now in particular on time. In other words, the background in the translational reference frame is not hydrostatic anymore since the frame moves relatively to the background. We conclude that stationary solutions can only exist in two disjoint cases:

C1 The reference frame does not move vertically, such that $C_z = 0$. In this case we find that $Z = \zeta$ and hence the background is again time-independent. We will refer to this case as horizontally traveling wave solution. It will be examined in §5.1.

C2 The background variables are constant in the first place and in general $C_z \neq 0$. If we combine the definition of the background temperature (2.15) with (2.17), we obtain

$$\frac{\kappa - 1}{\kappa} \frac{1}{T_0} = \eta_\rho + N^2. \quad (5.10)$$

From this brief calculation we can deduce that the background temperature must be constant if the rhs is constant. By this point we will refer to this case as isothermal traveling wave solution which will be investigated in §5.2.

In both cases, a stationary solution in the co-moving reference frame to (5.4) is given by

$$\Phi(\xi, \zeta) = K_x \xi + \int_{\zeta_0}^{\zeta} k_z(\zeta') d\zeta' \quad (5.11)$$

Where K_x is a constant being, without loss of generality, positive and k_z the root of the 4th order polynomial derived from the dispersion relation

$$(C_z k_z + (C_x - \hat{u}_{00}) K_x)^2 = \frac{N^2 K_x^2}{K_x^2 + k_z^2}. \quad (5.12)$$

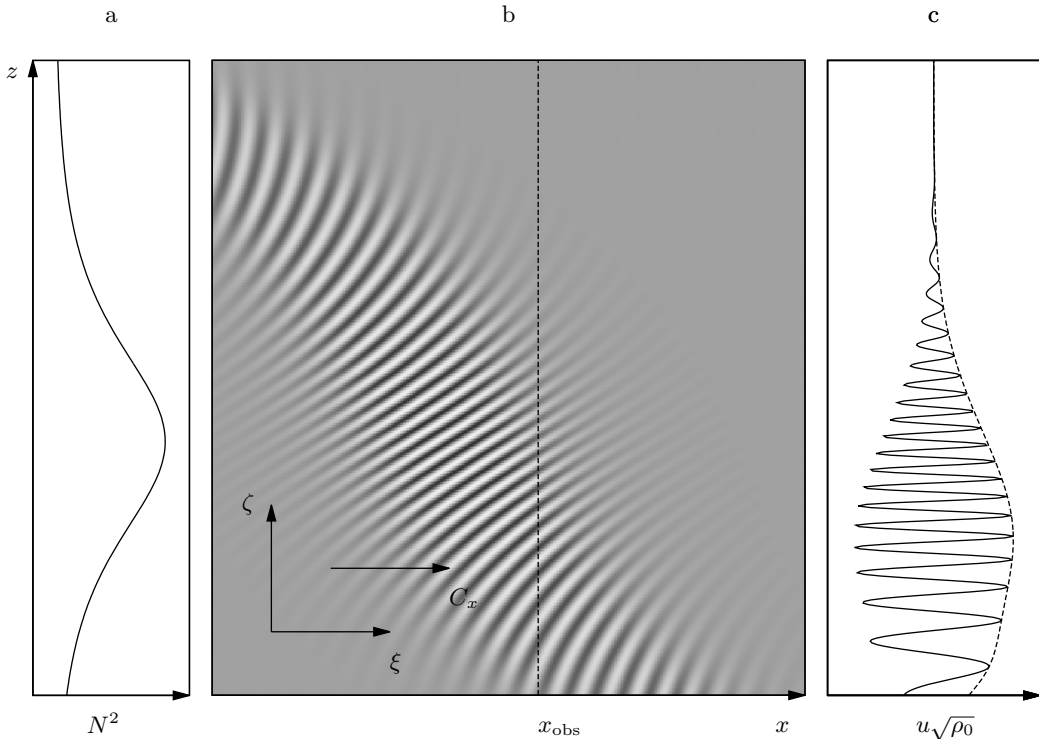


FIGURE 1. Illustration of the horizontally traveling wave solution without mean flow experiencing non-uniform stratification. Panel a: Squared Brunt-Väisälä frequency profile. Panel b: Horizontal wind component multiplied by the square root of the background density in the stationary coordinate system (x, z) . Also, the translational coordinate system (ξ, ζ) that moves with the constant velocity C_x to the right. Panel c: Profile that one would observe at x_{obs} .

The point ζ_0 denotes a reference point for the boundary conditions and may be chosen as $\zeta_0 = 0$, i.e. the bottom.

5.1. The horizontally traveling wave solution

In this section we want to investigate the horizontally traveling wave solution (C1), because it is possible to find analytic, explicit solutions in this case, even for arbitrary stratification. These solutions possess already some interesting properties such as non-linear phase and amplitude, as well as arbitrary mean flow horizontal wind.

If $C_z = 0$, then $\hat{u}_{0,0}$ disappears in (5.7), and hence (5.8) is solved by any real function

$$\hat{u}_{0,0}(\zeta) = u_{f0}(\zeta). \quad (5.13)$$

Although we did not show the equation, an evolution equation for $\hat{u}_{1,0}$ emerges at higher order in the asymptotic iteration. But fortunately, the same argument holds due to (5.9), so it turns out that $\hat{u}_{1,0}(\zeta) = u_{f1}(\zeta)$ is also an arbitrary function. Equation (5.12) reduces to a quadratic polynomial that is solved by

$$k_z(\zeta) = \pm \sqrt{\frac{N^2(\zeta)}{(C_x - u_{f0}(\zeta))^2} - K_x^2}. \quad (5.14)$$

It is worth pointing out that a negative discriminant results in an exponential growth or

decay of the wave in the vertical direction corresponding to a reflective layer. To prevent this, we constrain $N/K_x > |C_z - u_{f0}|$ at any point. Also, we must not have $u_{f0} = C_x$ at any point as it possibly causes singularities which corresponds to a critical layer.

To solve (5.5), we drop the time derivative and rewrite it as

$$\partial_\zeta G + \frac{c_{gx} - C_x}{c_{gz}} \partial_\xi G = 0 \quad (5.15)$$

which is an equation for the vertical wave action flux $G = \rho_0 c_{gz} a$. Its validity requires that $c_{gz} \neq 0$ which is fulfilled if $k_z \neq 0$ and bounded. This manipulation is feasible as c_g depends only on ζ due to (5.13) and (5.14). As soon as we find a solution for G , the amplitude can then be computed by $|A| = \sqrt{G\tilde{\omega}/(2\rho_0 c_{gz})}$. By the method of characteristics a solution is given by

$$G(\xi, \zeta) = G_0(\Psi) \quad (5.16)$$

with

$$\Psi(\xi, \zeta) = K_x \xi - K_x \int_{\zeta_0}^{\zeta} \frac{c_{gx}(\zeta') - C_x}{c_{gz}(\zeta')} d\zeta'. \quad (5.17)$$

The function G_0 can be determined by a boundary condition at ζ_0 . Equation (5.17) can be further simplified if we plug in the definition (3.31) and use the dispersion relation (5.4),

$$\Psi(\xi, \zeta) = K_x \xi - \int_{\zeta_0}^{\zeta} \frac{K_x^2}{k_z(\zeta')} d\zeta'. \quad (5.18)$$

Note that the characteristic curves given through Ψ are locally orthogonal on every line with constant phase Φ . This remarkable property will be investigated in detail in appendix B and used to construct the substitution that was postulated in order to obtain weak asymptotic solutions in §3 and appendix A. Taking advantage of (5.9) we can compute a solution to (5.6) by separation of variables, so

$$\arg(A)(\xi, \zeta) = L_\Psi \Psi(\xi, \zeta) - K_x \int_{\zeta_0}^{\zeta} \frac{u_{f1}(\zeta')}{c_{gz}(\zeta')} d\zeta' \quad (5.19)$$

with L_Ψ some constant which may be interpreted as a slow wavenumber. A general solution to (5.7) is found when inserting (5.5)

$$P_{0,0}(\xi, \zeta) = K_x (u_{f0}(\zeta) - C_x) a(\xi, \zeta) + P_f(\zeta) \quad (5.20)$$

with P_f some function.

Before we continue to derive an explicit, analytic solution, let us consider the energy budget. With the aid of (5.16) we can compute the energy exchange rate as presented in §4 as

$$q = K_x G \partial_Z u_{f0}. \quad (5.21)$$

If G is locally confined the energy exchange between wave and mean flow happens therefore on the characteristic curves defined by Ψ . And is strongest where the characteristic curve of the peak of G meets the level of strongest vertical shear.

We were able to derive a complete general solution in the case of a horizontally traveling wave. However, the solution is still not explicit since integrals emerged for Φ , Ψ and $\arg(A)$. They may be solved numerically. Though, for some particular background stratification profiles and horizontal mean-flow winds these integrals may have analytic solutions.

Consider a background with constant mean-flow, such that

$$u_{f0} = U_f = \text{const. and } u_{f1} = 0, \quad (5.22)$$

and a stratification profile

$$N^2(\zeta) = N_{\min}^2 + (N_{\max}^2 - N_{\min}^2) \left(1 + \left(\frac{\zeta - \zeta_0}{\Delta\zeta} \right)^2 \right)^{-2} \quad (5.23)$$

which represents a bell function with a peak of N_{\max}^2 centered at ζ_0 and width $\Delta\zeta$. For $\zeta \rightarrow \pm\infty$ it converges to N_{\min}^2 . When we insert these assumptions into (5.14), we obtain

$$k_z(\zeta) = \pm K_x \frac{\sqrt{N_{\max}^2 - N_{\min}^2}}{N_{\min}} \left(1 + \left(\frac{\zeta - \zeta_0}{\Delta\zeta} \right)^2 \right)^{-1}. \quad (5.24)$$

Here, we chose $C_x = N_{\min}/K_x + U_f$. It can be integrated by means of standard antiderivatives, so

$$\Phi(\xi, \zeta) = K_x \xi \pm K_x \Delta\zeta \frac{\sqrt{N_{\max}^2 - N_{\min}^2}}{N_{\min}} \arctan \left(\frac{\zeta - \zeta_0}{\Delta\zeta} \right) \quad (5.25)$$

and

$$\Psi(\xi, \zeta) = K_x \xi \mp K_x \Delta\zeta \frac{|N_{\min}|}{\sqrt{N_{\max}^2 - N_{\min}^2}} \left(\frac{\zeta - \zeta_0}{\Delta\zeta} + \frac{1}{3} \left(\frac{\zeta - \zeta_0}{\Delta\zeta} \right)^3 \right). \quad (5.26)$$

The slow phase becomes simply $\arg(A) = L_\Psi \Psi$.

In conclusion, for this particular stratification we found an analytic traveling wave solution. It is plotted in figure 1 for some choice of $O(1)$ -parameters and G_0 a bell function. This traveling wave is characterized by spatial modulation of phase as well as amplitude which is completely controlled by the stratification (see panel a). The structure is that of a locally confined wave packet. For $\Delta\zeta \rightarrow \infty$ the background tends to uniformity and the traveling wave merges to a plane wave. As the wave travels to the right, an observer at position x_{obs} (see panel b) would experience an upward propagating wave packet with downward traveling wave troughs and crests. As we decided for a constant mean-flow horizontal wind, there is no shear. So, there is no energy exchange between the wave and the mean-flow.

If $C_x = 0$, the result resembles a stationary wave in the original (X, Z) -coordinates. Such a wave can be interpreted as a mountain lee wave. The orography then may fix the boundary condition for G_0 . It is also possible to construct analytic traveling wave solutions in the same fashion, where $N = \text{const.}$, corresponding to an isothermal background, and $u_{f0}(\zeta)$ a prescribed profile. E.g., choosing $u_{f0}(\zeta) = u_0 + \Lambda\zeta$ linear provides also standard antiderivatives. Here, the energy exchange rate q is controlled by the constant shear Λ . This could be used to study the energy transport due to orography in circulation models.

5.2. The isothermal, horizontally periodic traveling wave

The previous section was dedicated to the horizontally traveling wave solutions *C1* where we found exact analytic solutions to the modulation equations. This section examines case *C2*, that is the isothermal traveling wave solutions, where the local Brunt-Väisälä frequency, N , and the logarithmic background derivative of the density, η_ρ , are constant. In this case a complete leading order solution of the scaled Euler equations cannot be achieved as we did not provide the explicit evolution equation for $\hat{u}_{1,0}$, which

is mandatory to compute $\arg(A)$ in (5.6). This is because the argument in (5.13), where $\hat{u}_{1,0}$ disappeared in the evolution equation, does not hold since in general we allow for a non-zero vertical relative velocity, $C_z \neq 0$. However, the remaining modulation equations are uncoupled, so they may possess some insightful solution.

Even though the 4th order polynomial in (5.12) has an analytic solution, its calculation does not provide any further enlightenment. We differentiate (5.4) instead w.r.t. ζ , which avoids lengthy terms and gives us an evolution equation for the vertical wave number. Closure of the system as well as substantial simplification can be gained if we restrict ourselves to horizontally periodic traveling waves, such that the horizontal derivatives in the modulation equations drop out. So, we may rewrite the modulation equations like

$$(\partial_\tau - C_z \partial_\zeta) k_z + \partial_\zeta (\hat{\omega} + K_x \hat{u}_{0,0}) = 0, \quad (5.27)$$

$$(\partial_\tau - C_z \partial_\zeta) a + (\partial_\zeta + \eta_\rho) (\hat{\omega}' a) = 0, \quad (5.28)$$

$$(\partial_\tau - C_z \partial_\zeta) \hat{u}_{0,0} = -(\partial_\zeta + \eta_\rho) (\hat{\omega}' K_x a). \quad (5.29)$$

The prime indicates the derivative w.r.t. k_z , such that $\hat{\omega}'(k_z) = c_{gz}(k_z)$.

This system has been studied numerically by Rieper *et al.* (2013a). A similiar system has been investigated by Dosser & Sutherland (2011). If we combine (5.28) with (5.29) and integrate, we obtain

$$\hat{u}_{0,0} = K_x a + u_0 \quad (5.30)$$

with $u_0 = u_0(\zeta + C_z \tau)$ being fixed by some boundary conditions. Injecting into (5.27), so

$$\partial_\tau k_z + \partial_\zeta (\hat{\omega} - C_z k_z + K_x^2 a + K_x u_0) = 0, \quad (5.31)$$

$$\partial_\tau a + \partial_\zeta ((\hat{\omega}' - C_z) a) = -\eta_\rho \hat{\omega}' a, \quad (5.32)$$

reduces the number of equations. As we seek for stationary solutions in the translational reference frame, we drop the time derivatives and constrain $u_0 = \text{const.}$, making it some mean-flow horizontal wind offset, to get rid of its τ -dependency. By that we can integrate (5.31) and solve for

$$a = \frac{\hat{\omega} - C_z k_z}{-K_x^2} + a_0. \quad (5.33)$$

The constant a_0 absorbed u_0 . Hereinafter, we handle $a = a(k_z)$ as function of k_z , so it becomes a diagnostic quantity. Inserting it into (5.32) yields a single, nonlinear, autonomous ODE for k_z , that can be written after some basic manipulation as

$$\partial_\zeta k_z = f(k_z) \text{ with } f(k_z) = \frac{2\eta_\rho}{K_x^2} \frac{\hat{\omega}'(k_z) a(k_z)}{a^{2''}(k_z)}. \quad (5.34)$$

The denominator of f occurred after differentiating (5.33) and using the identity

$$\frac{a^{2''}(k_z)}{2} = a'^2(k_z) + a(k_z) a''(k_z). \quad (5.35)$$

The ODE (5.34) has equilibrium solutions if the numerator of f vanishes, which happens either for $\hat{\omega}'(k_z^-) = 0$ or for $a(k_z^+) = 0$. By definition (3.31) it turns out that $k_z^- = 0$. Instead of solving (5.33) for k_z^+ , which means again finding the root of a quartic function, we can use it to fix its constant

$$a_0 = \frac{\hat{\omega}(k_z^+) - C_z k_z^+}{K_x^2}. \quad (5.36)$$

Both equilibria seem uninteresting at first glance: for k_z^+ the amplitude vanishes and for k_z^- there is no oscillation in the vertical, such that wave vector is purely horizontal. But maybe it exists some solution connecting asymptotically both equilibria which can then be considered as asymptotic rest states, such that

$$\lim_{\zeta \rightarrow \pm\infty} k_z = k_z^\pm. \quad (5.37)$$

Such a solution may be called wave front. Consider, without loss of generality, $k_z^+ < 0$ and an initial condition $k_z(0) = k_z^0 \in I = (k_z^+, k_z^-)$. We want to settle two questions: first, for which initial condition and set of parameters does a solution exist? And second, to which of the two asymptotic rest states does the solution converge? That is to determine the sign of f in (5.34). As we seek for upward propagating wave packets, we shall set $\text{sgn}(\hat{\omega}) = +1$, such that $\hat{\omega}' > 0$ on I . To guarantee that $|A| \in \mathbb{R}^+$, we must constrain $a > 0$ on I . In particular, we require $a(k_z^-) = a_- > 0$ which we can use to settle

$$C_z = \frac{\hat{\omega}(k_z^+) - N - K_x^2 a_-}{k_z^+}. \quad (5.38)$$

It emerges that $C_z > 0$, because we can estimate $\hat{\omega}(k_z^+) < N$ for all $k_z^+ < 0$. Our wave therefore always travels upwards. Note that by (2.18) and $\eta_T = 0$ (isothermal background), we get $\eta_\rho = -\kappa^{-1}N^2$. So, the numerator of f is negative on I . In order to obtain the sign of the denominator, we must consider (5.35) where

$$a'(k_z) = \frac{\hat{\omega}'(k_z) - C_z}{-K_x^2} \quad \text{and} \quad a''(k_z) = \frac{\hat{\omega}''(k_z)}{-K_x^2}. \quad (5.39)$$

If we evaluate (5.35) at $k_z^- = 0$, we find that

$$\frac{a^{2''}(k_z^-)}{2} = \frac{C_z^2}{K_x^4} + \frac{a_- N}{K_x^4} > 0. \quad (5.40)$$

As the denominator must not assume a root, a cannot have a saddle point on I . Neither, is a allowed to exhibit a local maximum, because $a^{2''}$ would switch sign and would particularly assume a root as it is continuous. The continuity of a prohibits also a local minimum, since it would imply a local maximum which we already ruled out. In conclusion, a must not have any critical points which yields the restriction $a' > 0$ on I , i.e. a is strictly increasing in k_z . This is fulfilled regarding (5.39) if $\hat{\omega}' < C_z$ on I . It turns out that

$$\arg \max_{k_z \in I} \hat{\omega}'(k_z) = \max \left(k_z^+, -\frac{K_x}{\sqrt{2}} \right). \quad (5.41)$$

This gives us a critical relative velocity for the existence of bounded traveling wave solutions

$$C_z^{\text{crit}}(k_z^+) = \begin{cases} \hat{\omega}'(-K_x/\sqrt{2}), & \text{if } k_z^+ < -K_x/\sqrt{2} \\ \hat{\omega}'(k_z^+), & \text{if } -K_x/\sqrt{2} \leq k_z^+ < 0 \end{cases} \quad (5.42)$$

where

$$\hat{\omega}'(-K_x/\sqrt{2}) = \frac{2}{3\sqrt{3}} \frac{N}{K_x}. \quad (5.43)$$

Demanding $C_z > C_z^{\text{crit}}(k_z^+)$ generates by (5.38) a lower bound on

$$a_- > a_-^{\text{crit}}(k_z^+) = \frac{\hat{\omega}(k_z^+) - k_z^+ C_z^{\text{crit}}(k_z^+) - N}{K_x^2}. \quad (5.44)$$

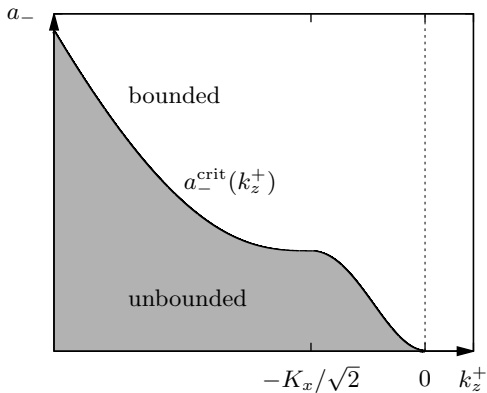


FIGURE 2. Critical asymptotic mass-specific wave action density. The isothermal traveling wave solutions cannot exist if the asymptotic rest states k_z^+ and a_- belong to the gray zone.

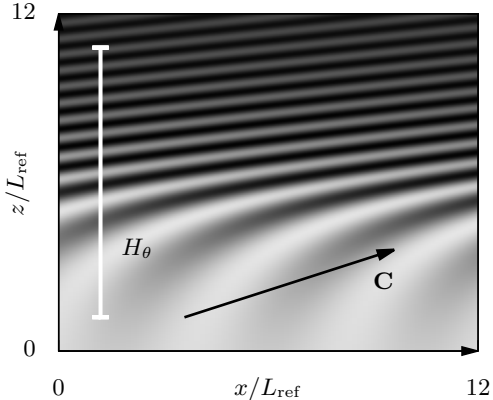


FIGURE 3. Illustration of the isothermal traveling wave front in two dimensions propagating with velocity \mathbf{C} . Horizontal wind u_* as given by (5.45). And the potential temperature scale height H_θ for comparison.

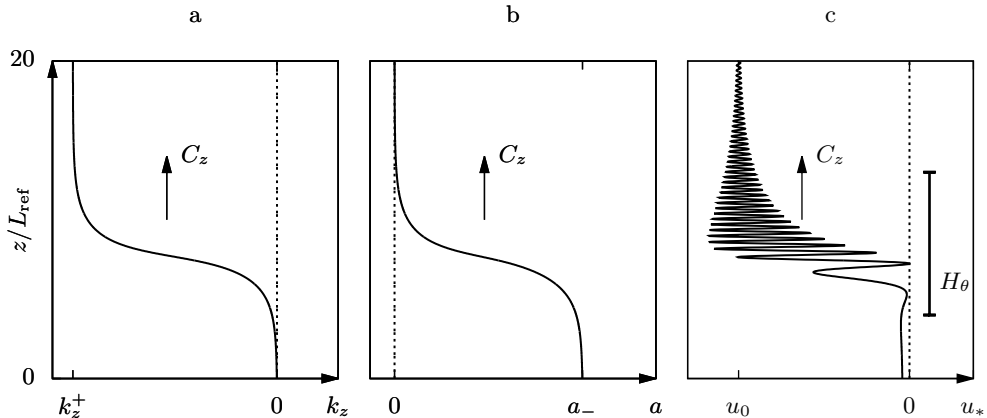


FIGURE 4. Illustration of the isothermal traveling wave front in one dimension. (panel a) Vertical wave number. (panel b) Mass-specific wave action density. (panel c) Horizontal wind as given by (5.45) and the potential temperature scale height H_θ for comparison.

The critical asymptotic mass-specific wave action density a_-^{crit} is illustrated in figure 2. Given that the previous constraints hold: by continuity $a^{2''}$ is positive on I and the sign of f is therefore negative. This means, for any $k_z^0 \in I$ the solution converges to the asymptotic rest state k_z^+ as $\zeta \rightarrow +\infty$. Vice versa, for $\zeta \rightarrow -\infty$ the solution tends to $k_z^- = 0$. So, as long as for some k_z^+ we choose a_- , such that it is in the white zone in figure 2, the solution converges. As soon as $a_- < a_-^{\text{crit}}$ (grey zone), the solution will run into a singularity and grow without bounds.

We want to point out that C_z is also the vertical component of the phase velocity. Multiplying by k_z gives us therefore the frequency in the stationary coordinate system. We may interpret (5.42) in terms of a critical frequency for a front-like traveling wave. In particular, for a lower boundary condition on k_z , that is an initial condition in the stationary system, this leads to a minimal frequency for the existence of traveling wave solutions.

| L_{ref}/km | H_{θ}/km | ε | N | K_x | a_- | k_z^+ | C_z |
|----------------------------|------------------------|---------------|-----|-------|-------|---------|-------|
| 3.053 | 30.53 | 0.1 | 1 | 1 | 1 | -1.3 | 1.1 |

 TABLE 2. $O(1)$ -parameters defining an isothermal, horizontally periodic traveling wave

The ODE (5.34) can be solved with the explicit Euler method. For some $O(1)$ -parameters (table 2), that fulfill the requirements, a particular solution illustrating the traveling wave front's properties is plotted in figure 4. Panel a shows the directly computed solution of the vertical wavenumber k_z , panel b has the mass-specific wave action density a diagnosed from (5.33), and panel c the leading order horizontal wind

$$u_* = \hat{u}_{0,0} + (\hat{u}_{0,1}e^{i\Phi\varepsilon^{-1}} + \text{c.c.}), \quad (5.45)$$

which is also shown in figure 3 from a two-dimensional perspective. We chose $u_0 = -K_x a_-$ for (5.30), so the mean-flow horizontal wind drops to zero after the front propagated through. To compute Φ from (5.11), we applied the very same Euler method. To compute $\hat{u}_{0,1}$ according to (3.24), we set $\arg(A) = \text{const.}$ because we lack an equation for it. The error produced by this oversimplification occurs in the wake of the front when k_z tends to zero, such that the slow phase $\arg(A)$ becomes vertically dominant and maybe produces some long wavelength vertical oscillation. From the two-dimensional point of view, the leading term in Φ is then still $K_x \xi$. However, this will not change the overall picture as the induced mean-flow regarding (5.30) is not affected by the slow phase. Again this traveling wave is characterized by spatial modulation of amplitude as well as phase.

The mass-specific wave action density and therefore the amplitude remain constant in the wake of the front. So at first glance, it seems like the wave induces wave energy into the mean flow. Because one would usually expect increasing amplitude with height due to the thinning air when the wave propagates upwards and due to the fact that the wave energy scales with the background density. This “extra” energy should then accelerate the mean-flow. This interpretation turns out to be incorrect, which becomes clear if we compute the wave-mean-flow energy exchange rate from §4 in the stationary (X, Z) -coordinate system,

$$q = K_x^2 \rho_0 a(k_z) \hat{\omega}'(k_z) a'(k_z) \partial_Z k_z < 0. \quad (5.46)$$

Here, we used (5.30) and the estimates from this section. We can already conclude that energy is exchanged directly in the front where the gradient is located. The rate is always negative. On the contrary, the wave gains energy from the mean flow and the mean-flow horizontal wind decelerates. This surprising behavior dissolves if we consider also the wave energy flux from (4.1). It tells us that the wave energy is transported with the group velocity $\hat{\omega}'$. But the front moves with C_z which is always greater than $\hat{\omega}'$ as we suppressed any critical points for a .

In summary, the fast traveling wave front only sustains if it obtains energy from the mean flow. One may ask if inverted traveling wave fronts possibly exist as solutions to the isothermal, horizontally periodic modulation equations. These would be solutions where the asymptotic rest states switched. So, $k_z^- \neq 0$ and $a_- = 0$ but $k_z^+ = 0$ and $a_+ \neq 0$. These solutions would be referred to as traveling wave backs. It turns out that backs cannot be solutions under no circumstances. We state this claim here unproved as the argumentation goes beyond the scope of this survey.

| L_{ref}/km | l_x/L_{ref} | l_z/L_{ref} | N_{min} | N_{max} | $\Delta\zeta$ | K_x | L_Ψ | $\Delta\Psi$ | G_{max} | $\text{sgn}(k_z)$ |
|----------------------------|----------------------|----------------------|------------------|------------------|---------------|-------|----------|--------------|--------------------|-------------------|
| 3.053 | 20 | 20 | 0.5 | 1.5 | 0.7 | 1.5 | -0.3 | 1.0 | 3×10^{-5} | -1 |

TABLE 3. Fixed parameters that define the traveling wave and experimental setup

6. Numerical validation of the traveling wave solutions under the full Euler dynamics

In the previous sections we found that traveling wave solutions for the modulation equations appear in two distinct cases. For the first case (*C1*), when the atmosphere is non-uniformly stratified, we were able to derive exact analytic solutions. The wave vectors can point in any direction but vertical. Though, the entire wave travels only in the horizontal direction. For the second case (*C2*), when the atmosphere is uniformly stratified (isothermal), we managed to show existence and the structure of the traveling wave solutions: assuming horizontal periodicity it occurs to be a front-like solution. These traveling waves propagate both horizontally and vertically. We found exact solutions to the modulation equations. But they are, however, asymptotic solutions to the fully nonlinear Euler equations. In this section we want to test the consistency of these solutions. The traveling wave solutions of the *C1*-case will be challenged numerically, so we can check the range of validity as the traveling wave solutions could be unstable intrinsically or only sustain for very small, even unrealistic ε . For this purpose, we will use a conservative solver of the Euler equations, the pincFloit model.

PincFloit stands for Pseudo-Incompressible Flow Solver with Implicit Turbulence and was introduced by Rieper *et al.* (2013*b*). This finite-volume flow solver conserves energy, momentum as well as mass and suits therefore the purpose well. Within the framework of the model it is possible to simulate with almost unconstrained background stratifications apart from the uniform, weakly stratified atmosphere. The fidelity of the model was tested against standard cases. Rieper *et al.* (2013*a*) applied pincFloit to check the range of validity of the extended WKB theory for gravity waves of Achatz *et al.* (2010) which provides the basis for our traveling wave solutions. Recently, Muraschko *et al.* (2015); Bölöni *et al.* (2016) derived a numerical solver for the modulation equations based on a Lagrangian ray-tracing approach for horizontally homogeneous GW packets that was also tested with the aid of pincFloit. It discretizes the governing equations on an equidistant staggered C-grid. From the alternative schemes, that the model provides, it proved practical to apply the third order, low storage Runge-Kutta time stepping scheme, which is total variation diminishing. This is combined with the MUSCL scheme for spatial discretization and a monotonized central flux limiter. As the name of the model implies, it is capable of solving the compressible Navier-Stokes equations. But since this survey is only interested in the Euler equations, any diffusion or dissipation are switched off.

We validate the *C1* traveling wave solution with non-uniform stratification as given by the equations (5.22)-(5.26). They are not compactly supported on the two-dimensional domain. Inevitably, the wave will touch the boundary of the computational domain. In order to prevent reflection, we prescribe the analytic solution on the boundary cells for all times. We choose a particularly challenging test case such that the background stratification and the amplitude varies like $O(1)$ on the whole domain. The mean-flow horizontal wind is chosen in a way that the horizontal translational, relative velocity C_x vanishes, so

$$U_f = -N_{\text{min}}/K_x. \quad (6.1)$$

By this choice the traveling wave is stationary in the fix coordinate system, such that $(\xi, \zeta) = (X, Z)$, which makes it convenient to compare the initial condition with the final state. The wave amplitude is set to be of the same order as the mean flow to provoke nonlinear coupling. So, the setup can be viewed as a wave that wants inherently to migrate towards the right side with a constant horizontal group velocity but faces an opposing wind of the exact same velocity. If the model manages to balance these tendencies the outcome stands at rest.

The parameters that define the traveling wave and the background are presented in table 3. They were chosen in a way that they resemble a typically unresolved wave in weather and climate models. Here, l_x and l_z are the domain size in x- and z-direction, respectively. The initial wave action flux is given by a bell shaped function

$$G(X, Z) = G_{\max} \left(1 + \left(\frac{\Psi(X, Z) - \Psi(X_{\text{pos}}, Z_{\text{pos}})}{\Delta\Psi} \right)^4 \right)^{-2} \quad (6.2)$$

where G_{\max} is the maximum flux at the peak.

To prescribe the stratification in the model, we have to provide the background density, Exner pressure, and potential temperature. The latter can be computed by means of standard antiderivatives from (5.23). The background Exner pressure is defined through the hydrostatic equation (2.13) which we must integrate numerically. This is achieved by a simple Euler forward scheme with very high resolution. It looks costly at first glance but it only needs to be computed once at start.

Deviations between simulation and theory are measured by the weighted norms of the numerically simulated field (num) minus the analytically expected (true) field. Hereinafter, we consider the horizontal wind field as we did not find any significant differences from the other fields in terms of errors. We define the weighted error norms as

$$\begin{aligned} l_1 &= \frac{I(|u_{\text{true}} - u_{\text{num}}|)}{I(|u_{\text{true}}|)} \\ l_2 &= \left(\frac{I(|u_{\text{true}} - u_{\text{num}}|^2)}{I(|u_{\text{true}}|^2)} \right)^{1/2} \\ l_\infty &= \frac{\max_{x,z}(|u_{\text{true}} - u_{\text{num}}|)}{\max_{x,z}(|u_{\text{true}}|)} \end{aligned} \quad (6.3)$$

where I denotes the numerical approximation to the integral

$$I(u) \approx \int_0^{l_x} \int_0^{l_z} u(x, z) dz dx. \quad (6.4)$$

The numerical quadrature exploits the trapezoidal rule.

In order to test the consistency of the traveling wave solutions, the scale separation parameter ε is altered whereas all other parameters, as given in table 3 determining the properties of the traveling wave, are kept constant. The analytical asymptotic solution in non-dimensional form can be written as

$$U_{\text{true}} = \hat{U}_{0,0} + \left(\hat{U}_{0,1} e^{i\varepsilon^{-1}\Phi} + \text{c.c.} \right) + O(\varepsilon) \quad (6.5)$$

for $\varepsilon \rightarrow 0$ and (X, Z, T) fixed. We call the solution is consistent if we can reproduce the analytically expected order of convergence from (3.1) of $M = 1$ numerically for a broad

| H_θ/km | ε | $t_{\text{end}}^*/\text{s}$ |
|----------------------|---------------|-----------------------------|
| 45.57 | 0.067 | 1204 |
| 37.23 | 0.082 | 889 |
| 30.53 | 0.100 | 660 |
| 25.03 | 0.122 | 490 |
| 20.35 | 0.150 | 360 |

TABLE 4. Varying parameters for the experiments testing the consistency of the traveling wave.

range of ε . In §2 we defined

$$\varepsilon = \frac{L_{\text{ref}}}{H_\theta}. \quad (6.6)$$

As we vary ε , we keep L_{ref} fixed, such that the spatial resolution per wave period remains constant. This choice provides the benefit that we do not need to adapt the resolution for each value of ε . If we did so, then we could not distinguish effects on the error of the varying ε from the varying resolution. All experiments were performed with a resolution of 256×512 grid cells, which corresponds to approximately 18 grid cells per wave period which is a reasonable value to resolve all important features.

As we change ε from one experiment to another, we must constrain that $T = \varepsilon t = O(1)$, which fulfills a necessity of the asymptotic ansatz, and hence the dimensionful overall simulation time must change like

$$t_{\text{end}}^* = O\left(\frac{t_{\text{ref}}}{\varepsilon}\right) = O\left(\varepsilon^{-2/3}\right) \quad \text{since} \quad t_{\text{ref}} = \sqrt{H_\theta/g} = O(\varepsilon^{-1/2}). \quad (6.7)$$

Table 4 presents the parameters defining each of the five experiments. In particular, the simulation time t_{end}^* is shown in the rightmost column. The potential temperature scale height varies from roughly 20 to 46 km throughout the simulations which gives us a considerable range for the scale separation.

The simulation results are plotted in figure 5. The stratification, horizontal wind, and its relative deviation from the analytic solution are depicted for three of the experiments. For smallest $\varepsilon = 0.067$ (top row) the stratification is moderate and the amplitude envelope, which is given by the wave action flux G , is also rather broad in width. The horizontal wind oscillates around a mean flow of about 12 ms^{-1} with an amplitude of 3 ms^{-1} .

The lines of constant phase are nearly straight, so are the characteristic lines Ψ , which define the shape of the envelope. With even smaller ε the wave will get closer to the uniformly stratified regime with infinitesimal amplitude which can be captured by the Boussinesq theory. The relative error after the simulation is as expected very small, much less than 1% at the peaks. Remarkably, the error is almost perfectly in phase with the initial wave at least in the middle of the domain. This means that errors are not generated by non-stationary effects. The wave does not move at all, the peaks are slightly smeared out, probably, by some numerical dissipation. By increasing ε , the width of the stratification peak narrows. Also, the envelope confines and its maximum increases. The mean-flow horizontal wind gets stronger and we can expect nonlinear effects.

For $\varepsilon = 0.1$ (second row) the mean flow approaches 15 ms^{-1} and the horizontal wind varies with an amplitude of about $\pm 10 \text{ ms}^{-1}$ which produces some substantial shear. In this case, we observe clearly some error sources at the upper boundary. These are

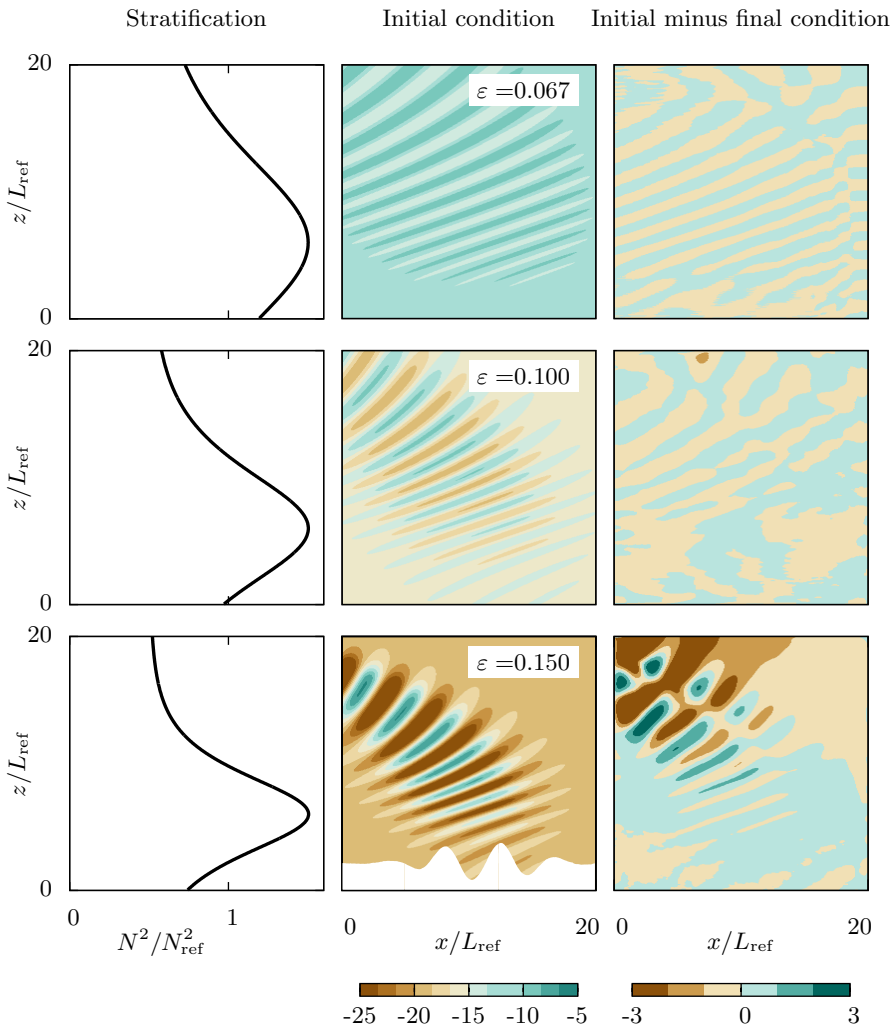


FIGURE 5. Computational corroboration of the existence of horizontally traveling wave solutions. (left column) Stratification represented by the local squared Brunt-Väisälä frequency. (middle) Initial total horizontal wind u_{true} in ms^{-1} . (right) Deviation between the numerical and the approximate asymptotic solutions after simulation time t_{end}^* (see table 4). i.e. $u_{\text{true}} - u_{\text{num}}$. (middle column, bottom row) The filled white curve depicts a stream line being inflated by a factor 64.

numerical errors. As we prescribe the expected analytic solution at the boundaries, even small deviations of the numerical solution in the domain can cause discontinuities directly at the boundary. These shocks then propagate into the domain.

For even higher ε , nonlinear effects start to dominate the error production. In the experiment where $\varepsilon = 0.15$ (third row), the mean-flow is about 18 ms^{-1} and the horizontal wind oscillates with an amplitude of about 40 ms^{-1} which is not captured by the color scale of figure 5 anymore. Here, we find some quadrupole structure in the relative error field that indicates phase shifts by some instability process which are triggered most likely by the boundary discontinuities. The local error exceeds 3 ms^{-1} at some points.

For this particular case we also plotted a stream line at the bottom in figure 5 which is

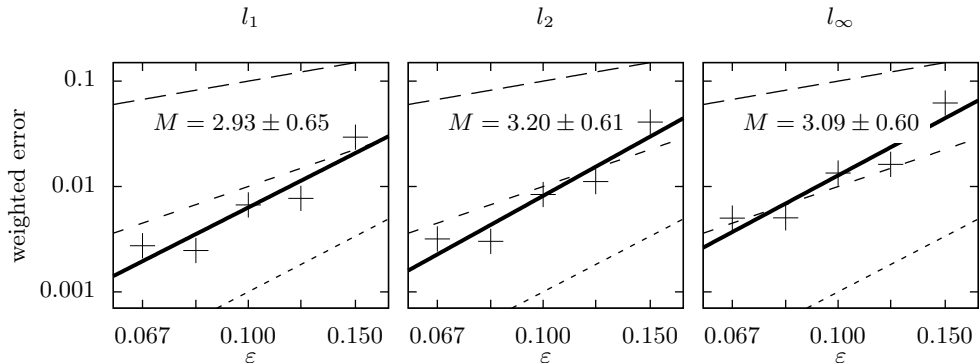


FIGURE 6. Convergence of the error norms with regard to ε . (solid line) Linear regression on a log-log scale applying the least square method reveals an order of convergence M and its standard deviation. (long dashed) first order, (medium dashed) second order, and (short dashed) third order lines.

amplified for better visibility. This line represents just as well a mountain ridge of about 200 m height that could have excited the wave.

For all five experiments, we computed the error norms according to (6.3). The results are shown in figure 6 where we plotted the error norms against ε on a log-log scale. A least square fit gives us the order of convergence M assuming that the error norms converge like

$$l_n = C\varepsilon^M \quad \text{for } n = 1, 2, \infty. \quad (6.8)$$

We also computed its standard deviation which are depicted aside the fitted lines in figure 6. For all three norms we obtain convergence like $O(\varepsilon^3)$. Even after subtracting the rounded error margin of 1 from the order, it is apparently still included in the expected $O(\varepsilon)$ -convergence with a comfortable cushion. For larger ε the model probably overestimates the norms due to the numerical errors at the boundaries propagating into the domain and triggering instabilities. We tested the influence of this effect by changing the integration domain of the norms like

$$I(u) \approx \int_{\delta}^{l_x - \delta} \int_{\delta}^{l_z - \delta} u(x, z) dz dx \quad (6.9)$$

and δ some positive fixed number. So, we focus on a smaller box and ignore cells that are potentially influenced by the boundaries. For some values of δ we recalculated the error norms for every ε . There was no significant effect on the order of convergence. So either the hypothesis of boundary discontinuities propagating into the domain causing instabilities is wrong or they already contaminate the whole domain after the simulation time as they propagate faster than expected or instabilities are excited by other processes. This remains an open question.

However, for small ε the norms are presumably also overrated as the amplitudes become so small that nonlinear coupling between the wave and the mean flow becomes inefficient and numerical damping takes over. Taking these effects into account, with an order of convergence of about three, we can safely conclude that the traveling waves are consistent for a significant parameter range.

7. Hydrostatic gravity waves

In the previous section, we showed that the horizontally traveling wave solutions (C1) resemble stationary mountain lee waves at least qualitatively. In the numerical experiments though, we used rather small wavelengths of about 3km both vertical and horizontal. As the overall motivation of this survey is to lay the foundation for more realistic instability criteria in gravity wave parametrizations, the natural choice to test the asymptotic consistency of the traveling wave solutions was to use typically unresolved small wavelengths. But mountain waves in nature are mostly hydrostatic waves, i.e. they exhibit much longer horizontal than vertical wavelengths, such that their dynamics are anisotropic. For the derivation of the modulation equations we assumed a non-hydrostatic, isotropic scaling. This section is concerned with the question whether our modulation equations and their traveling wave solutions still apply in the hydrostatic limit.

In this regard Achatz *et al.* (2010, 2017) showed that the consistency between the scale asymptotics of the Euler equations and the pseudo-incompressible equations also holds for hydrostatic gravity waves. Bölöni *et al.* (2016) investigated the non-hydrostatic modulation equations numerically applying a ray-tracer method. The model was validated, among others, by initializing hydrostatic waves with a horizontal to vertical wavelength ratio of 10. The results were compared with reference simulations computed with pincFloit (Rieper *et al.* 2013b). Both models were in excellent agreement.

Based on these considerations we will rescale the Euler equations (2.19) for hydrostatic gravity waves and solve them asymptotically with the spectral WKB method presented in §3. We assume a horizontal to vertical wavelength ratio to be $O(\varepsilon)$ whereas the same distinguished limit provided in §2 shall hold. In particular, the vertical wavelength is small in comparison to the scale height and the background varies slowly with respect to the fast oscillations. In order to capture the anisotropic dynamics, we introduce rescaled coordinates

$$(X, Z, T) = (\varepsilon^2 x, \varepsilon z, \varepsilon^2 t) \quad (7.1)$$

and consider the following ansatz for the WKB approximation

$$\begin{pmatrix} \mathbf{v} \\ \theta \\ \pi \end{pmatrix} = \begin{pmatrix} u_\varepsilon^{(0)}(x, z, t; \varepsilon) \\ \varepsilon w_\varepsilon^{(1)}(x, z, t; \varepsilon) \\ \theta_0(Z) + \varepsilon \theta_\varepsilon^{(1)}(x, z, t; \varepsilon) \\ \pi_0(Z) + \varepsilon^2 \pi_\varepsilon^{(2)}(x, z, t; \varepsilon) \end{pmatrix}. \quad (7.2)$$

Note that, in contrast to (7.2), the vertical wind occurs at $O(\varepsilon)$ (cf. Achatz *et al.* 2010) whereby all the other symbols have their usual meaning. If we insert (7.2) into the Euler equations (2.1) and substitute by

$$U = (u, w, B, P)^T := \left(u_\varepsilon^{(0)}, \varepsilon w_\varepsilon^{(1)}, \frac{1}{N} \frac{\theta_\varepsilon^{(1)}}{\theta_0}, \theta_0 \pi_\varepsilon^{(2)} \right)^T, \quad (7.3)$$

then we can exploit the series expansion (3.1) combined with the WKB assumption

$$(X, Z, T) \mapsto \hat{U}_{n,m}(X, Z, T), \quad \Phi(X, Z, T). \quad (7.4)$$

By the weak asymptotic approach of appendix A we can order terms in powers of ε and thereby obtain to leading order a homogenous linear system for the primary harmonics

$\mathbf{M}\hat{U}_{0,1} = 0$ with the coefficient matrix

$$\mathbf{M}(-i\hat{\omega}_h, \mathbf{k}) = \begin{pmatrix} -i\hat{\omega}_h & 0 & 0 & ik_x \\ 0 & 0 & -N & ik_z \\ 0 & N & -i\hat{\omega}_h & 0 \\ ik_x & ik_z & 0 & 0 \end{pmatrix}. \quad (7.5)$$

The intrinsic frequency for the hydrostatic waves is found to be by $\hat{\omega}_h = \omega - k_x \hat{u}_{0,0}$ where ω and \mathbf{k} are the time and spatial derivatives of the phase Φ , respectively. The homogenous system for $\hat{U}_{0,1}$ has non-trivial solution only if $\det(\mathbf{M}(-i\hat{\omega}_h, \mathbf{k})) = 0$, which yields the dispersion relation

$$\hat{\omega}_h^2 = \frac{N^2 k_x^2}{k_z^2}. \quad (7.6)$$

The kernel of \mathbf{M} provides the polarization relation $\mathcal{U} \in \ker(\mathbf{M})$ which turns out to be the same as the non-hydrostatic (3.23), so that the solution can be written as

$$\hat{U}_{0,1} = A\mathcal{U}(\hat{\omega}_h, \mathbf{k}) \quad (7.7)$$

with $A \in \mathbb{C}$ being the scalar amplitude. To leading order, we also get constraints for the mean flow

$$\hat{w}_{0,0} = 0, \quad \hat{B}_{0,0} = 0, \quad \text{and} \quad \partial_X \hat{u}_{0,0} = 0. \quad (7.8)$$

At the next order, we obtain an inhomogeneous system for the primary harmonics being of the same form as (3.17) with only a change in the linear differential operator

$$\mathbf{L}(\delta_T, \nabla_\varepsilon) = \begin{pmatrix} \delta_T & \partial_Z \hat{u}_{0,0} & 0 & \partial_X \\ 0 & 0 & 0 & \partial_Z - N^2 \\ 0 & 0 & \delta_T & 0 \\ \partial_X & \partial_Z + N^2 + \eta_\rho & 0 & 0 \end{pmatrix}. \quad (7.9)$$

Multiplying the inhomogeneous equation from the left by the conjugate transpose of the kernel vector and adding its complex conjugate, we obtain a conservation law,

$$\partial_T \mathcal{A} + \nabla_\varepsilon \cdot (\mathbf{c}_{gh} \mathcal{A}) = 0, \quad (7.10)$$

for the wave action density $\mathcal{A} = \rho_0 |A|^2 / \hat{\omega}_h$ which constitutes an equation of motion for the absolute wave amplitude $|A|$. By subtracting its complex conjugate, we get an equation of motion for the argument of the amplitude

$$(\partial_T + \mathbf{c}_{gh} \cdot \nabla_\varepsilon) \arg(A) = -k_x \hat{u}_{1,0}. \quad (7.11)$$

The hydrostatic group velocity is given by

$$\mathbf{c}_{gh} = \frac{\partial \hat{\omega}_h}{\partial \mathbf{k}} + \hat{u}_{0,0} \mathbf{e}_x. \quad (7.12)$$

Also at the next order, we find the very same equation of motion for the non-hydrostatic mean-flow horizontal wind (3.34) which can be recast with the aid of the hydrostatic polarization (7.7) to

$$\rho_0 \left(\partial_T \hat{u}_{0,0} + \partial_X \hat{P}_{0,0} \right) = -\nabla_\varepsilon \cdot ((\mathbf{c}_{gh} - \hat{u}_{0,0} \mathbf{e}_x) k_x \mathcal{A}). \quad (7.13)$$

In conclusion, we find hydrostatic modulation equations (7.10), (7.11), and (7.13) that differ from the non-hydrostatic ones (3.32), (3.33), and (3.38) only due to the dispersion relation (7.6). If we perform a Taylor expansion of the non-hydrostatic dispersion relation

(3.22) for $|k_x| \ll |k_z|$ in the variable k_x/k_z , i.e. assuming steep wave vectors (Bühler 2009, p 121), we obtain

$$\hat{\omega} = \hat{\omega}_h + O(|k_x/k_z|^2). \quad (7.14)$$

Therefore, we deduce that the non-hydrostatic modulation equations also hold in the hydrostatic limit. This statement also implies that the traveling wave solutions, which we found for the non-hydrostatic case, are equally valid for large horizontal wavelength or small K_x , accordingly. The result is of particular interest for the *C1*-class since it demonstrates that they indeed describe typical mountain lee waves.

8. Conclusion

We started our derivations from the dimensionless, fully compressible Euler equations. By assuming low Mach number, leading order stable stratification, non-hydrostatic motion, and a large internal Froude number, we found a distinguished limit similar to Achatz *et al.* (2010). The scale separation parameter ε , which is now the only parameter appearing in the equations, is the ratio of the dominant wavelength and the scale height.

The scaled Euler equations were derived from a multiple scale ansatz that divided the wave from a hydrostatic background. We combined a spectral expansion approach with the WKB assumption of slow modulation of amplitude and phase. So, the frequency and wave numbers are defined locally as the temporal and spatial derivatives of the phase, respectively. Since the system is nonlinear and we allowed for wave-mean-flow interaction, even the leading order equations are contaminated by higher harmonics.

Instead of an averaging technique (e.g. Grimshaw 1974; Tabaei & Akylas 2007) that assumes *a priori* periodicity of the asymptotic solution with respect to the fast phase, we applied the more general approach presented in Danilov *et al.* (2003) of weak asymptotic solutions.

Investigating the results of the asymptotic analysis leads to the modulation equations: equations of motion for the phase, wave action density, and the leading order mean-flow variables. These equations are in line with the findings of Achatz *et al.* (2010). But in addition to that we found an evolution equation for the argument of the complex valued amplitude and a constraint for the higher-order mean-flow horizontal wind which becomes necessary to close the equation system. Computing the energy budget revealed that these equations conserve the sum of wave and mean-flow energy.

We found two distinct classes of traveling wave solutions for the modulation equations: the horizontally traveling wave solution and the isothermal traveling wave solution. For the former, we were able to construct analytic solutions. The horizontally traveling wave solution with $C_x = 0$ may be applied to model mountain lee waves for arbitrary stratification, background horizontal wind, and orography. Typically, mountain lee waves are hydrostatic. Although the modulation equations were derived for non-hydrostatic gravity waves, it was shown that they also hold in the hydrostatic limit where the wave vector becomes steep. With the additional assumption that the wave is horizontally periodic, we investigated the existence and the shape of the isothermal traveling wave solution. It resembles an upward propagating wave front. Quite surprisingly, the isothermal traveling wave front decelerates the mean flow in order to sustain its constant amplitude.

The horizontally traveling waves were validated numerically against the fully nonlinear Euler equations. Exact solutions of the modulation equations fulfill the Euler dynamics asymptotically. The purpose of the numerical simulations was to clarify the consistency of the solutions, i.e. range of validity of the asymptotic approximation. The traveling wave solutions performed surprisingly well: they exceeded the analytically expected order of

convergence of one, as the scale separation parameter tends to zero. The numerically computed order turned out to be around three. This result holds on a broad range of scale separation parameters which proves the consistency of the traveling wave solutions presented in this survey.

In a companion paper we will analyze the traveling waves, that we found here, with respect to stability by analytical and numerical methods.

The authors thank the German Research Foundation (DFG) for partial support through the research unit Multiscale Dynamics of Gravity Waves (MS-GWaves) and through grants AC 71/8-1, AC 71/9-1, AC 71/10-1, and KL 611/25-1. M.S. thanks Gergely Bölöni for vital support with pincFloit.

Appendix A

This appendix introduces the weak asymptotic scheme which allows to successively iterate the asymptotic solution in order to achieve an equation hierarchy. Our objective is to establish that the coefficients $\mathcal{C}_{k,l}$ from (3.7) vanish independently of k and l . This is usually achieved by an orthogonality argument that the harmonics are mutually orthogonal with respect to the inner product given by the average over the interval $[0, 2\pi]$ w.r.t. the fast phase $\varepsilon^{-1}\Phi$ (Miura & Kruskal 1974; Grimshaw 1974; Tabaei & Akylas 2007). There are two issues with this approach: First, the fast phase does depend on ε , such that the phase lines squeeze together when ε tends to zero. Second and most importantly, Φ is actually a function of space and time, therefore solving the integral requires an integration by substitution. We can circumnavigate these issues if we seek for asymptotic solutions in a weak sense (Danilov *et al.* 2003). Consider a differentiable, compactly supported test function S . We want to multiply S together with some test harmonic $\exp(-im\varepsilon^{-1}\Phi)$ to (3.7) and integrate over the entire real line with regard to the phase Φ . The aforementioned substitution must be an injective, continuously differentiable mapping, say

$$(X, Z, T) \mapsto F(X, Z, T) \quad (\text{A } 1)$$

which is independent of ε with $F = (\Phi, \Psi, \tau)$. We will present a particular mapping of this kind in appendix B. The weak formulation of (3.7) reads then

$$\sum_{k=0}^M \sum_{|l| \leq k+2} \varepsilon^k \int_{\mathbb{R}} S(\Phi) (\mathcal{C}_{k,l} \circ F^{-1})(\Phi, \Psi, \tau) e^{i(l-m)\varepsilon^{-1}\Phi} d\Phi + o(\varepsilon^M) = 0. \quad (\text{A } 2)$$

Holding τ and Ψ constant, we call (3.1) a weak asymptotic solution if it fulfills (A 2) for all $m \in \mathbb{N}$ and all well-behaved S . We may rewrite (A 2) for the forthcoming argument as

$$\sum_{k=0}^M \varepsilon^k \int_{\mathbb{R}} S \left(\mathcal{C}_{k,m} \circ F^{-1} + \sum_{\substack{|l| \leq k+2 \\ l \neq m}} (\mathcal{C}_{k,l} \circ F^{-1}) e^{i(l-m)\varepsilon^{-1}\Phi} \right) d\Phi + o(\varepsilon^M) = 0. \quad (\text{A } 3)$$

One can show via integration by parts that the sum over l in (A 3) vanishes like $O(\varepsilon)$ when ε tends to zero, as

$$\int_{\mathbb{R}} S(\mathcal{C}_{k,l} \circ F^{-1}) e^{i(l-m)\varepsilon^{-1}\Phi} d\Phi = -\frac{\varepsilon}{i(l-m)} \int_{\mathbb{R}} \frac{\partial (S(\mathcal{C}_{k,l} \circ F^{-1}))}{\partial \Phi} e^{i(l-m)\varepsilon^{-1}\Phi} d\Phi = O(\varepsilon). \quad (\text{A } 4)$$

Here, we exploited that S has compact support. The existence of the integral requires that $\mathcal{C}_{k,l}$ is differentiable which translates to the ansatz functions and background variables that their second derivative must also exist. With (A 4) we can safely apply the limit $\varepsilon \rightarrow 0$ for (A 3) and iterate the solution: The sum over l in (A 3), i.e. the second summation, does not contribute to the leading order due to (A 4), such that $\mathcal{C}_{0,m} = 0$ for all m and S . In the next order these terms appear, but we can insert the leading order solution and find that they cancel out, such that also $\mathcal{C}_{1,m} = 0$ for all m and S . We can successively proceed to order $o(\varepsilon^M)$. To put it in a nutshell, the scaled Euler equations (2.19) possess weak asymptotic solutions in the limit $\varepsilon \rightarrow 0$ of the form (3.1) only if $\mathcal{C}_{k,m} = 0$ holds for all possible k and m .

Appendix B

This appendix investigates the existence of weak asymptotic solutions as introduced in §3 and appendix A. We already stated in §5.1 that the characteristic curves (5.18) are locally orthogonal on every line with constant phase Φ . This motivates to introduce a curvilinear, translational, orthogonal coordinate system $\Theta = (\Phi, \Psi, \tau)$ via $(\xi, \zeta, \tau) \mapsto \Theta(\xi, \zeta, \tau)$. The orthogonality can be proven when we write down the contravariant local basis vectors,

$$\mathbf{e}_\Phi = \frac{K_x}{\|\mathbf{k}\|} \mathbf{e}_x + \frac{k_z}{\|\mathbf{k}\|} \mathbf{e}_z \quad \text{and} \quad \mathbf{e}_\Psi = \frac{k_z}{\|\mathbf{k}\|} \mathbf{e}_x - \frac{K_x}{\|\mathbf{k}\|} \mathbf{e}_z, \quad (\text{B } 1)$$

that we obtain from computing the Jacobian of the coordinate transformation Θ . It becomes now obvious that $\mathbf{e}_\Phi \cdot \mathbf{e}_\Psi = 0$ which proves the orthogonality. Since $k_z \neq 0$ is restricted, its sign cannot change and hence the integrals in (5.11) and (5.18), which determine Φ and Ψ , respectively, are monotone, continuous, and especially injective. The mapping $F = \Theta \circ \Gamma(X, Z, T)$ fulfills therefore the requirements for the substitution presented in appendix A. The existence of such a mapping was at this point only postulated. As (5.11) holds also for the isothermal traveling wave solution (C2), we can construct the curvilinear transformation there as well. So, this brief appendix justifies in hindsight the validity of the weak asymptotic scheme.

REFERENCES

- ACHATZ, U. 2007 Gravity-wave breaking: Linear and primary nonlinear dynamics. *Adv. Sp. Res.* **40**, 719–733.
- ACHATZ, U., KLEIN, R. & SENF, F. 2010 Gravity waves, scale asymptotics and the pseudo-incompressible equations. *J. Fluid Mech.* **663**, 120–147.
- ACHATZ, U., RIBSTEIN, B., SENF, F. & KLEIN, R. 2017 The interaction between synoptic-scale balanced flow and a finite-amplitude mesoscale wave field throughout all atmospheric layers: weak and moderately strong stratification. *Q. J. R. Meteorol. Soc.* **143** (702), 342–361.
- ALEXANDER, M. J. & DUNKERTON, T. J. 1999 A spectral parameterization of mean-flow forcing due to breaking gravity waves. *J. Atmos. Sci.* **56** (24), 4167–4182.
- BALDWIN, M.P., GRAY, L.J., DUNKERTON, T.J., HAMILTON, K., HAYNES, P.H., RANDEL, W.J., HOLTON, J.R., ALEXANDER, M.J., HIROTA, I., HORINOUCHE, T., JONES, D.B.A., KINNERSLEY, J.S., MARQUARDT, C., SATO, K. & TAKAHASHI, M. 2001 The Quasi-Biennial Oscillation. *Rev. Geophys.* **39** (2), 179–229.
- BECKER, E. 2012 Dynamical control of the middle atmosphere. *Space Sci. Rev.* **168** (1–4), 283–314.
- BÖLÖNI, G., RIBSTEIN, B., MURASCHKO, J., SGOFF, C., WEI, J. & ACHATZ, U. 2016 The interaction between atmospheric gravity waves and large-scale flows: an efficient description beyond the non-acceleration paradigm. *J. Atmos. Sci.* **73** (12), 4833–4852.

- BÜHLER, O. 2009 *Waves and mean flow*, 1st edn. New York: Cambridge University Press.
- CHU, V. H. & MEI, C. C. 1970 On slowly-varying Stokes waves. *J. Fluid Mech.* **41**, 873–887.
- DANILOV, V. G., OMELYANOV, G. A. & SHELKOVICH, V. M. 2003 Weak asymptotics method and interaction of nonlinear waves. In *Asymptot. methods wave quantum Probl.*, 208th edn. (ed. M. V. Karasev), pp. 33–163. Amer. Math. Soc., Providence, RI.
- DAVIES, T., STANFORTH, A., WOOD, N. & THUBURN, J. 2003 Validity of anelastic and other equation sets as inferred from normal-mode analysis. *Q. J. R. Meteorol. Soc.* **129**, 2761–2775.
- DOSSER, H. V. & SUTHERLAND, B. R. 2011 Weakly nonlinear non-Boussinesq internal gravity wavepackets. *Phys. D Nonlinear Phenom.* **240** (3), 346–356.
- FRITTS, D. C. 2003 Gravity wave dynamics and effects in the middle atmosphere. *Rev. Geophys.* **41**, 1–64.
- GRIMSHAW, R. 1974 Internal gravity waves in a slowly varying, dissipative medium. *Geophys. Fluid Dyn.* **6**, 131–148.
- KLEIN, R. 2011 On the Regime of Validity of Sound-Proof Model Equations for Atmospheric Flows. In *ECMWF Workshop on Non-Hydrostatic Modelling, November 2010*. <http://www.ecmwf.int/publications/library/do/references/list/201010>.
- KLEIN, R., ACHATZ, U., BRESCH, D., KNIO, O. M. & SMOLARKIEWICZ, P. K. 2010 Regime of validity of soundproof atmospheric flow models. *J. Atmos. Sci.* **67** (10), 3226–3237.
- LELONG, M.-P. & DUNKERTON, T. J. 1998 Inertia-gravity wave breaking in three dimensions. Part I: convectively stable waves. *J. Atmos. Sci.* **55** (1997), 2473–2488.
- LIU, W., BRETHERTON, F. P., LIU, Z., SMITH, L., LU, H. & RUTLAND, C. J. 2010 Breaking of progressive internal gravity waves: convective instability and shear instability. *J. Phys. Oceanogr.* **40**, 2243–2263.
- LOMBARD, P. N. & RILEY, J. J. 1996 Instability and breakdown of internal gravity waves. I. Linear stability analysis. *Phys. Fluids* **8** (12), 3271–3287.
- MCCLANDRESS, C. 1998 On the importance of gravity waves in the middle atmosphere and their parameterization in general circulation models. *J. Atmos. Solar-Terrestrial Phys.* **60** (14), 1357–1383.
- MIED, R. P. 1976 The occurrence of parametric instabilities in finite-amplitude internal gravity waves. *J. Fluid Mech.* **78**, 763–784.
- MIURA, R. M. & KRUSKAL, M. D. 1974 Application of a nonlinear WKB method to the Korteweg-DeVries equation. *SIAM J. Appl. Math.* **26** (2), 376–395.
- MURASCHKO, J., FRUMAN, M. D., ACHATZ, U., HICKEL, S. & TOLEDO, Y. 2015 On the application of Wentzel-Kramer-Brillouin theory for the simulation of the weakly nonlinear dynamics of gravity waves. *Q. J. R. Meteorol. Soc.* **141** (688), 676–697.
- RIEPER, F., ACHATZ, U. & KLEIN, R. 2013a Range of validity of an extended WKB theory for atmospheric gravity waves: one-dimensional and two-dimensional case. *J. Fluid Mech.* **729**, 330–363.
- RIEPER, F., HICKEL, S. & ACHATZ, U. 2013b A conservative integration of the pseudo-incompressible equations with implicit turbulence parameterization. *Mon. Weather Rev.* **141** (3), 861–886.
- SUTHERLAND, B. R. 2001 Finite-amplitude internal wavepacket dispersion and breaking. *J. Fluid Mech.* **429**, 343–380.
- SUTHERLAND, B. R. 2006 Weakly nonlinear internal gravity wavepackets. *J. Fluid Mech.* **569**, 249–258.
- TABAEI, A. & AKYLAS, T. R. 2007 Resonant long-short wave interactions in an unbounded rotating stratified fluid. *Stud. Appl. Math.* **119** (3), 271–296.
- WHITHAM, G. B. 1965 A general approach to linear and non-linear dispersive waves using a Lagrangian. *J. Fluid Mech.* **22** (2), 273–283.